Deltares

SBW Wave overtopping and grass cover strength

Predictions of Prototype Tests Nijmegen Millingen aan de Rijn

Gijs Hoffmans (Deltares)
Jentsje van der Meer (Van der Meer Consulting)
Joep Frissel (Alterra)
Maurice Paulissen (Alterra)
Henk Verheij (Deltares)
Gosse Jan Steendam (Infram)

1206016-007

Deltares

Title
SBW Wave overtopping and grass cover strength

Client	Project	Reference	Pages
Rijkswaterstaat Waterdienst	1206016-007	1206016-007-GEO-0004-gbh	42

Trefwoorden
Wave overtopping, erosion, grass, sod, wave run-up
golfoverslag, golfoploop, erosie, grasbekleding, grastrekproef, graskwaliteit

Samenvatting
Wave overtopping and grass cover strength is part of the project SBW Wave overtopping and revetment strength (SBW: Strength of and loads on water defenses), or 'SBW Golfoverslag en Sterkte Bekledingen' in Dutch. The project is one part of the SBW research program to develop the safety assessment tools for primary water defenses in The Netherlands. The program is funded by the Dutch ministry of Environment and Infrastructure, delegated to Rijkswaterstaat Waterdienst (Dutch) and, again, delegated to Deltares, the independent research institute on delta technology.

In the past five years, 2007-2012, research was carried out to determine the grass cover strength in case of wave overtopping. The research resulted in a Technical Report (ENW 2012). Tests were carried out with the wave overtopping simulator (WOS) on several Dutch and Belgium dikes in the winter season. A closed grass sod proved to be very resilient against the erosive forces of massive wave overtopping volumes. On the other hand rough herbal growth and open patches in the sod can make it vulnerable to erosion.

From 2007 to 2012 the research was not conclusive on the effect of objects and transitions from slope to berm and transitions from a grass cover to other (hard) revetment types. Also the wave run-up zone was not yet covered. The report at hand starts a next research period which will take until 2017 and where the aim will be to incorporate the aspects noted above.

This report contains the 'prediction' step for the river dikes at the locations Millingen and Nijmegen. The following aspects about erosion of grass are covered: evaluation of the visited sites for conducting the prototype experiments in the winter period 2012-2013; load predictions with respect to the cumulative load (distributions of the overtopping wave volumes according to the new theory of Hughes et al. 2012 are discussed); sod cover and root density investigations for predicting the grass strength; prediction of the critical depth-averaged flow velocity (U_c) for grass covers at two locations i.e. in Millingen and at the Hollands-Duits pumping station in Nijmegen.

Versie	Datum	Auteur	Paraaf	Review	Paraaf	Goedkeuring	Paraaf
	Feb. 2013	Gijs Hoffmans		Mark Klein Breteler		Leo Voogt	

State
Final

Contents

1 Introduction

1.1 Framework and research approach

Wave overtopping and grass cover strength is part of the project SBW Wave overtopping and revetment strength (SBW: Strength of and loads on water defenses), or 'SBW Golfoverslag en Sterkte Bekledingen' in Dutch. The project is one part of the SBW research program to develop the safety assessment tools for primary water defenses in The Netherlands. The program is funded by the Dutch ministry of Environment and Infrastructure, delegated to Rijkswaterstaat Waterdienst (Dutch) and, again, delegated to Deltares, the independent research institute on delta technology.

In 2007 a project group was formed to study and answer the research questions concerning the grass cover strength in case of wave overtopping. Deltares, Van der Meer Consulting, Inframa and Alterra participate herein.

In the past five years, 2007-2012, research was carried out to determine the grass cover strength in case of wave overtopping. The research resulted in a Technical Report (ENW 2012). Tests were carried out with the wave overtopping simulator (WOS) on several Dutch and Belgium dikes in the winter season. A closed grass sod proved to be very resilient against the erosive forces of massive wave overtopping volumes. On the other hand rough herbal growth and open patches in the sod can make it vulnerable to erosion.

From 2007 to 2012 the research was not conclusive on the effect of objects and transitions from slope to berm and transitions from a grass cover to other (hard) revetment types. Also the wave run-up zone was not yet covered. The report at hand starts a next research period which will take until 2017 and where the aim will be to incorporate the aspects noted above.

The research questions concerning grass erosion are approached in a cyclic way (Figure 1.1 www.thesis.nl/kolb). The current report 'Prediction' uses the models and methods to make a prediction and perform an experiment (wave overtopping test). The next step will be to describe the state of the art models and ways to enhance insight in the process of erosion of grass around objects and transitions. Evaluation of the prediction and experimental results will lead to better models and methods.

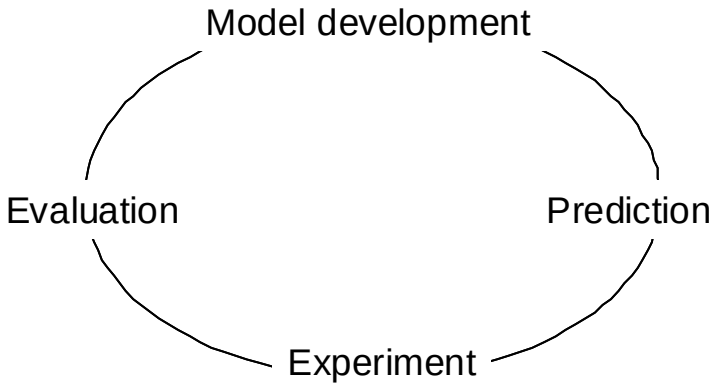

Figure 1.1 Cyclic research approach

In the period until 2017 two cycles are foreseen, followed by an update of the Technical Report. Foreign readers are welcomed to use the research results generated within the SBW program. This is the main reason to report in English. Interaction and feedback on the use of the results are appreciated. It must be noted that the prediction models and experiences picked up by testing with the wave overtopping simulator are based on the Dutch and (some) Belgium circumstances, grasses and substrates. Grasses and substrate may be very similar in the wider region. However, on a global scale species composition and climatic conditions may vary strongly, possibly causing differences in behavior of grass revetments on dikes.

Foreign readers are welcomed to use the research results generated within the SBW program, but to contact Deltares or Rijkswaterstaat Waterdienst if they choose to do so. This is the main reason to report in English. Interaction and feedback on the use of the results are appreciated. It must be noted that the prediction models and experiences picked up by testing with the wave overtopping simulator are based on the Dutch and (some) Belgium circumstances, grasses and substrates. Grasses and substrate can be very similar in the wider region, however, they can also differ.

1.2 Readers guidance

This report contains the 'prediction' step in the cyclic research approach, especially for river dikes. The following aspects about erosion of grass are covered:

- Chapter 2 briefly evaluates the visited sites for conducting the prototype experiments in the winter period 2012-2013.
- Chapter 3 deals with the load predictions. Distributions of the overtopping wave volumes according to the new theory of Hughes et al. 2012 are discussed. Moreover, predictions with respect to the cumulative load are made.
- Chapter 4 gives an overview of the sod cover and root density investigations for predicting the grass strength.
- Chapter 5 describes the prediction of the critical depth-averaged flow velocity (U_c) for grass covers at two locations i.e. in Millingen and at the Hollands-Duits pumping station in Nijmegen. This prediction is based on root tensile-stress tests (root properties; lower boundary) and grass sod tensile-stress tests (soil properties; upper boundary).
- Appendices A to F give additional information about the state of the art modelling of the grass strength.

2 Test locations

On Tuesday (16 May 2012) several locations were visited and evaluated for conducting wave-overtopping tests in the winter 2012-2013. These experiments aim to understand the failure mechanism of grass revetments, especially near objects and transitions. Moreover, they are needed for validating “the state of the art” models.

Mr. Kapinga of the Waterboard ‘Rivierenland’ prepared the visit by choosing a number of locations between Nijmegen and the German border. They are

1 Fish ladder near Hollands Duits pumping-station (EN 102).
2 Road on crest of dike, berm and connection to bank consisting of gras-betonstenen bij wiel EN 098.
3 Road on crest of dike, landward slope 1V:2.5H - 1V:3H – horizontal (EN 049).
4 High situated berm and trees (EN 040).
5 Road on crest of dike (EN 025).

Below some comments are made for planning the experiments. At location 1 the erodibility of grass near obstacles/transitions can be tested. At location 5 there is a road on the crest of the dike. Here diversion of traffic is easy to achieve. Moreover, water is available from the nearby pond. When 3 to 4 tests are planned per location, the locations 1 (Photo 1) and 5 are preferable. The locations 2, 3 and 4 were evaluated as being less interesting for testing. For example, no interesting obstacles were present and/or the public road on the crest had to be closed during testing and/or no sufficient water supply was present.

Photo 2.1 Fish ladder near Hollands Duits pumping-station (overview of location 1)

Relevant remarks with respect to location 1 are:

- Closing the road is not necessary.
- Wave-overtopping simulator can be positioned on the crest near the road.

- Water is available from the fish ladder.
- Strip 1 is along the concrete structure. At the bottom, there is a transition of a trail and a concrete beam which puts out the soil surface.
- Strip 2 is towards the concrete beam on which a vertical wall can be positioned. In this way, the erodibility of grass near a big object can be simulated.

Photo 2.2 Concrete roof of fish ladder (Location 1), Inner side of the dike is on the left

Photo 2.3 Connection of concrete roof of fish ladder to grass cover (Location 1)

Photo 2.4 Piling sheet at the bottom of strips 1 and 2 (Location 1)

Photo 2.5 Trail between piling sheet and transition of slope to berm (Location 1)

Photo 2.6 Detail of concrete beam. To simulate the erosion of grass near a big obstacle (Location 1) a vertical structure could be positioned (Photo 7)

Photo 2.7 Vertical structure

Relevant remarks with respect to location 5 are:

- The road on the crest near EN 024 - EN025 is designed for local traffic and therefore easy to cut off temporarily.
- On the left side of the pond, the road changes in a bike-way.
- The edges of the road are damaged. The erodibility can be tested.
- Near the pond at the toe of the dike there is a drainage system consisting of gravel.

Photo 2.8 Road on the crest (EN 025) (Overview of location 5)

Photo 2.9 Road on the crest, on the right there is a pool (Location 5)

Photo 2.10 Road on the crest, damage is severe close to the asphalt (Location 5)

3 Wave overtopping

3.1 New distribution of overtopping wave volumes

The distribution of overtopping wave volumes till now was described by a Weibull distribution with a fixed shape factor of b = 0.75. This distribution has been used for all the overtopping tests so far and results in very large overtopping wave volumes if a significant overtopping discharge is assumed. Sometimes the maximum overtopping wave volume was calculated as 20-40 m^3 per m width, which is actually more than a real overtopping wave can contain.

It was already argued in the Design Report (2009) for the US Overtopping Simulator and also in Van der Meer et al. (2010), based on the work of Hughes and Nadal (2009), that for very large overtopping the b-value in the Weibull distribution was likely to increase. The Weibull distribution is given by

$$P_V = P(\underline{V} \le V) = 1 - \exp\left[-\left(\frac{V}{a}\right)^b\right] \tag{3.1}$$

The development in theory over the last two years is given in Hughes et al. (2012).

If "b" varies also "a" will vary, where "a" and "b" had a simple relationship for b = 0.75. The relationship is written as

$$a = \left(\frac{1}{\Gamma(1+\frac{1}{b})}\right)\left(\frac{qT_m}{P_{ov}}\right) \tag{3.2}$$

where Γ is the mathematical gamma function.

Hughes et al. (2012) gives for b the following relationship (Fig. 3.1)

$$b = \left[exp\left(-0.6\frac{R_c}{H_{m0}}\right)\right]^{1.8} + 0.64 \tag{3.3}$$

Figure 3.1 shows that for $R_c/H_{m0} > 1.5$ the average value of b is indeed about 0.75, but that with smaller crest freeboard the b-value may increase significantly, leading to a gentler distribution of overtopping wave volumes. A comparison of old and new theory is shown in Figure 3.2.

Calculation of the real overtopping wave volumes for a test for simulation has shown that it is necessary to adjust the a-value, if the number of overtopping waves is small. The adjustment is required to match the total volume of the overtopping waves with the average discharge in the given test duration. This adjustment needs to be established and this has been performed with a similar analysis as for a constant b-value of 0.75. The following equation has to be used to calculate the correct a-value

$$a = \left[\left(\frac{1}{\Gamma(1+\frac{1}{b})} + 1.6{N_{ow}}^{-0.75} - 0.009\right)\right]\left(\frac{qT_m}{P_{ov}}\right) \tag{3.4}$$

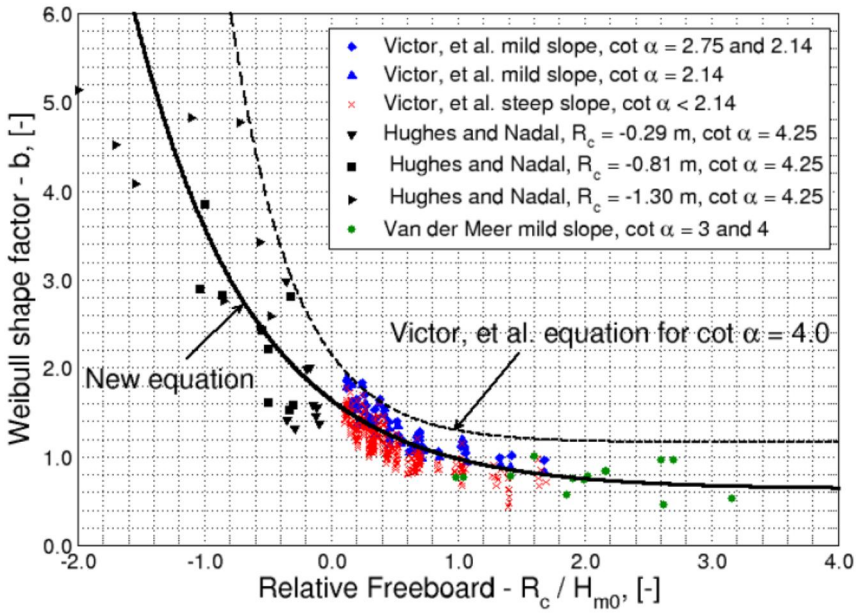

Figure 3.1 New Weibull shape factor, b, spanning a large range of relative freeboard (Hughes et al. (2012)

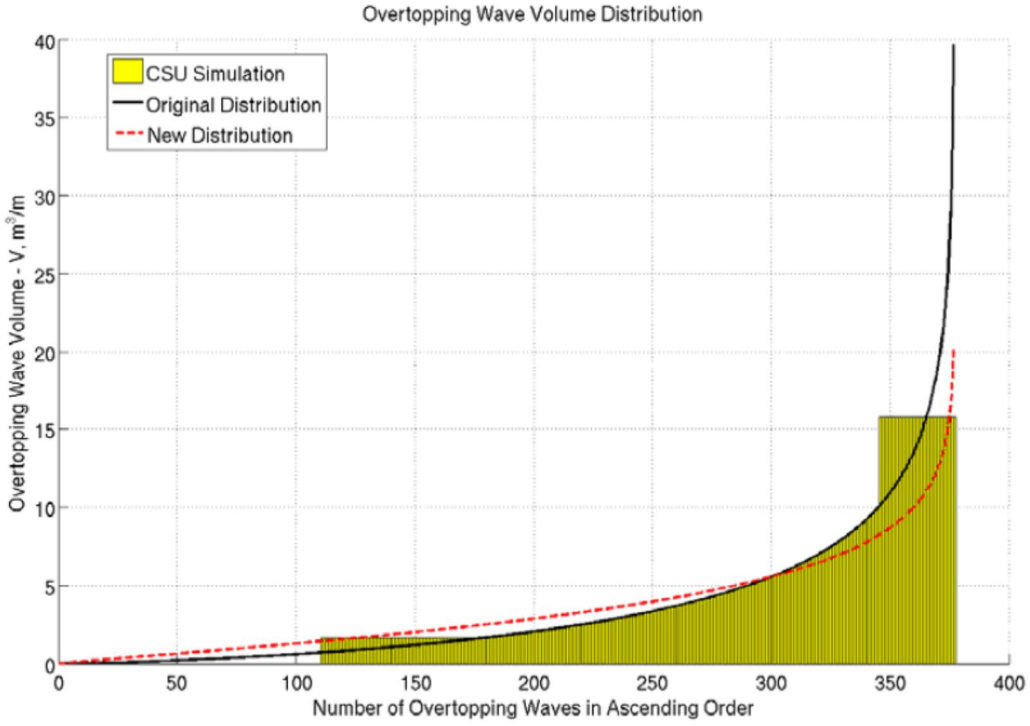

Figure 3.2 Wave overtopping distribution for simulating q = 370 l/s per m, old and new theory (Hughes et al. 2012).

The difference in a-value between Equations 3.2 and 3.3 is given by $1.6N_{ow}^{-0.75}$-0.009 and is shown in Figures 3.3 and 3.4 for a small and a large number of overtopping waves. The data points were derived from all test conditions for the Jacksonville tests in August 2012, for q = 0.01 cfs/ft up to q = 4 cfs/ft (similar to about 1 to 400 l/s per m).

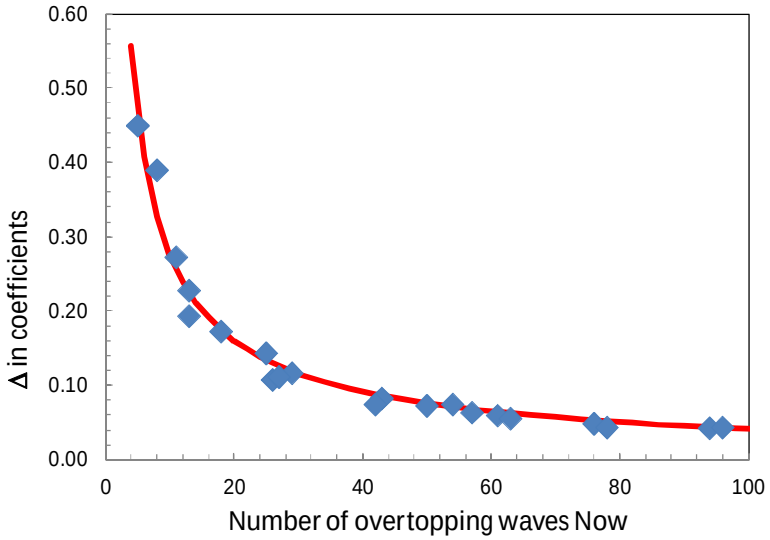

Figure 3.3 Adjustment of a-value for N_{ow} < 100

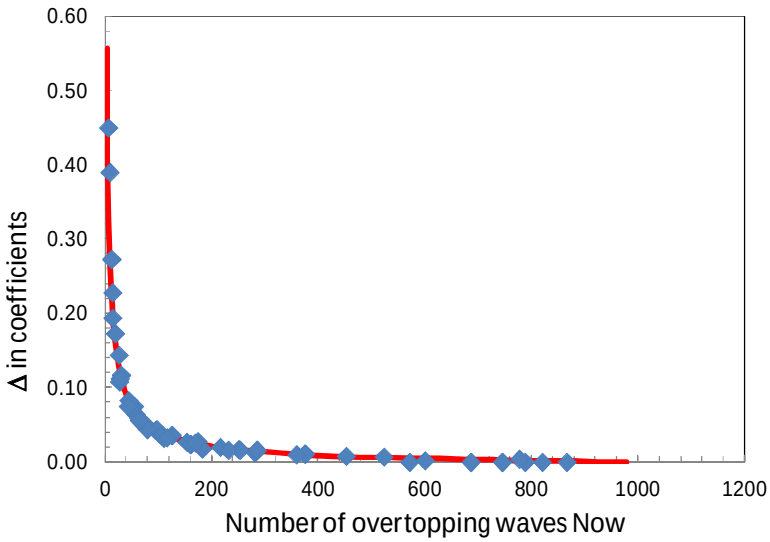

Figure 3.4 Adjustment of a-value for N_{ow} < 1000

3.2 Overtopping distributions for tests at Nijmegen

The new tests at Nijmegen will be performed on a river dike. As for the tests at river dikes in Belgium in 2010, a lower wave height has to be assumed than what has been used now for sea and lake dikes. Wave heights at a river dike are seldom larger than 1 m and for a similar discharge they will give more, but smaller, overtopping waves than for a wave height of 2 m.

The new distribution for overtopping waves will also give less significant overtopping waves than before, certainly when the overtopping discharge will become large. For example, with a wave height of 1 m (two hours duration), the old theory gives a maximum overtopping wave volume of 6.3 m^3 per m for an average overtopping discharge of 100 l/s per m. This volume exceeds the capacity of the overtopping simulator (5.5 m^3 per m) and actually an overtopping discharge of 100 l/s per m is the limit for simulation, using the old theory. Using the new theory gives b = 1.16 instead of 0.75 and the maximum overtopping volume becomes now

2.4 m^3 per m, which is less than half of the original value. If the overtopping discharge is increased to 200 l/s per m, the maximum overtopping wave volume is 11.6 m^3 per m with the old theory and 3.6 m^3 per m with the new theory. This is more than a factor 3 difference.

Assuming a wave height of H_s = 1 m, a wave steepness of s_{op} =0.04 new distributions of wave overtopping volumes have been made, which should be used for testing at the river dikes at Nijmegen. Figure 3.5 gives distributions for q = 0.1 and 1 l/s per m for a duration of 6 hours and distributions for q = 5, 10, 30, 50, 75, 100, 150 en 200 l/s per m for a duration of 2 hours.

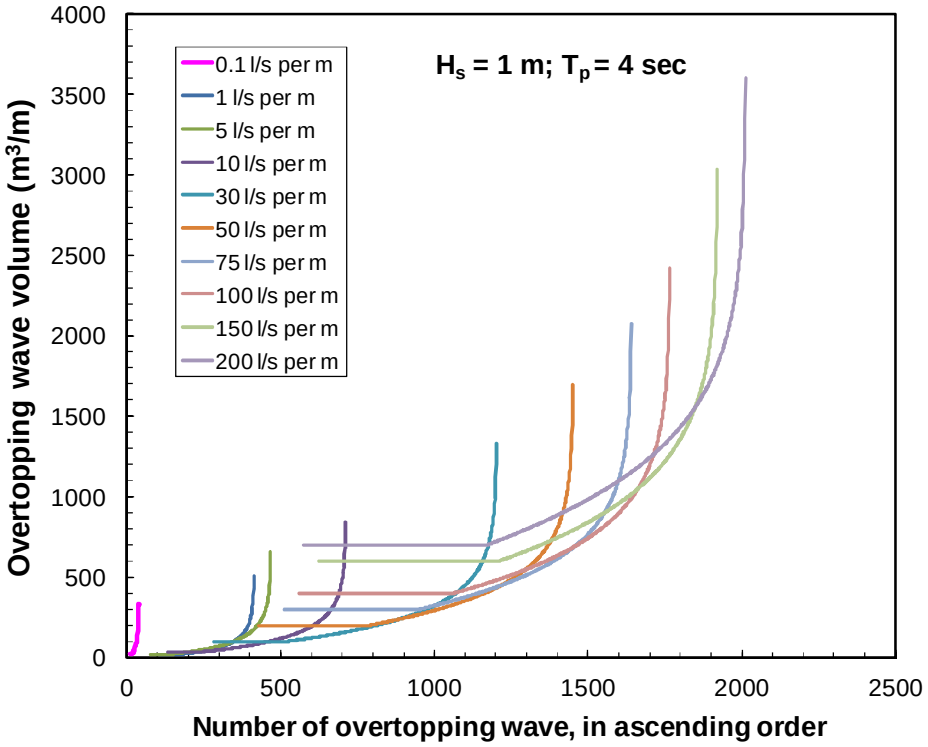

Figure 3.5 Distributions of overtopping wave volumes according to the new theory (H_s = 1 m, T_p = 4.0 s, cotα = 3)

The given overtopping distributions have effect for the tests to come. The normal procedure considered overtopping discharges for six hours and in a sequence of 1, 10, 30, 50 en 75 l/s per m. The overtopping discharge of 75 l/s per m was seen as the maximum capacity of the wave overtopping simulator, assuming a wave height of 2 m. With the new theory and a lower wave height the maximum overtopping discharge may become 200 l/s per m or more.

This has two consequences. The first is that a new set of consecutive overtopping discharge has to be chosen. A sequence may be q = 1 (speeded up); 10; 50; 100 and 200 l/s per m. This gives again about 5 tests of 6 hours, where the first test will be speeded up by applying a larger discharge (but the correct overtopping wave volumes). The second consequence is that till now pumps have been used of about 100 l/s per m capacity. To double this discharge could mean that the pump capacity has to be doubled (including all the hoses). Another solution is to perform the test two times slower, using a filling discharge of 100 l/s per m, but simulating the correct overtopping wave volumes for 200 l/s per m. This increases the total test duration by exactly 6 hours.

3.3 Cumulative overload for tests at Nijmegen

3.3.1 Cumulative overload at the crest

Recently, the overload method is developed

$$\sum_{i=1}^{N}\left(U_i^2 - U_c^2\right) = D$$

where N is the number of the largest waves for $U > U_c$, U is the flow velocity (related to the wave) and U_c is the critical flow velocity. In order to make a prediction for the tests at Nijmegen the cumulative overload for each test and for the accumulation of tests, has to be established. First of all this will be done at the crest, directly after release of the overtopping wave volume from the wave overtopping simulator. The velocities and flow thicknesses that are produced by the simulator are known, see SBW report (2012). In the same report also the theory for steady state overflow at a slope has been described and compared with measured velocities and flow thicknesses. Although the friction factor varies from 0.01 to 0.1 (see SBW report 2012 Model development) it was concluded that by using a friction factor of f = 0.01 in the theoretical formulae gave a good reproduction of the measured values. These formulae will then be used to give the cumulative overload further down the slope. Note that in Millingen the flow velocities and flow depths will be measured at two locations on the slope to validate the proposed value of f = 0.01.

The flow velocity and thickness at the crest can be given by:

$U = 4.5\ V^{0.3}$ (u in m/s; V in m^3/m; coefficient 4.5 is not dimensionless) (3.5)

$h = 0.1\ V^{0.75}$ (h in m; V in m^3/m; coefficient 0.1 is not dimensionless) (3.6)

Velocities can be calculated with Equation 3.5 for all overtopping wave volumes as given in Figure 3.5. And then the cumulative overload can be calculated for various critical velocities u_c. Table 3.1 gives the cumulative overload for critical velocities at the crest for critical velocities of u_c = 4, 5 and 6.3 m/s (values used in earlier analysis) and for single tests with the given overtopping discharge and for a *duration of 1 hour*.

q	0.1	1	5	10	30	50	75	100	150	200
	l/s per m	l/s per m	l/s per m	l/s per m	l/s per m	l/s per m	l/s per m	l/s per m	l/s per m	l/s per m
uc=4 m/s				2	36	127	335	648	1542	2812
uc=5 m/s						2	14	43	180	461
uc=6.3 m/s										5

Table 3.1 Cumulative overload (m^2/s^2) for various discharges and critical velocities and for a duration of 1 hour (assuming H_s = 1 m). Location: at the crest

By assuming a test sequence q = 1, 10, 50, 100 and 200 l/s per m and with a subtest duration of 6 hours it is also possible to calculate the total cumulative overload after each subtest, including the previous subtests. The data in Table 1 have been used for this and the results are shown in Table 3.2. If a critical velocity of u_c =6.3 m/s is assumed, there will hardly be any overload.

q	1	10	50	100	200
	l/s per m	l/s per m	l/s per m	l/s per m	l/s per m
uc=4 m/s		12	774	4662	21534
uc=5 m/s			12	270	3036

Table 3.2 Total cumulative overload (m^2/s^2) for a sequence of 5 subtests with various critical velocities and for a duration of 6 hours for each subtest (assuming H_s = 1 m). Location: at the crest

Based on clay and grass investigation it might be possible to predict a critical velocity for the section to be tested. With such a critical velocity one can predict when first damage, more open spots and failure should occur, where it is noticed that only failure is the most reliable prediction for

$$\Sigma(u^2 - u_c^2) = 3500 \text{ m}^2/\text{s}^2$$

3.3.2 Cumulative overload at 10 m down a 1:3 slope

The SBW-report (2012) clearly showed that velocities increased significantly down a 1:2.4 slope (Tholen), where they remained more or less similar for a gentler slope of about 1:5 (Vechtdike). The slopes at Nijmegen in average are close to a 1:3 slope. As this is not too far from a 1:2.4 slope it is expected that velocities at the crest of the dike will increase along the 1:3 slope. The length of the slopes at Nijmegen varies, but each of them has at least a length of 10 m. As velocities along the slope are expected to increase, the cumulative overload will also increase. This is a reason why often the damage was found at the second half down the slope and not close to the crest.

The theory of steady state overflow, as described in the SBW-report (2012) can be used to calculate the velocities down a 1:3 slope, using f = 0.01. Velocities which are higher than 4 m/s may contribute to the cumulative overload for a critical velocity of u_c = 4 m/s. Velocities of 7 m/s will only be reached for the largest overtopping wave volumes that are possible from the simulator. Therefore velocities u_o at the crest have been chosen of u_o = 4; 5; 6 and 7 m/s. Then the theoretical formulae have been used to calculate the velocities along a 1:3 slope. Figures 3.6 – 3.9 give the results for the given velocities at the crest, including the calculation for the flow thickness.

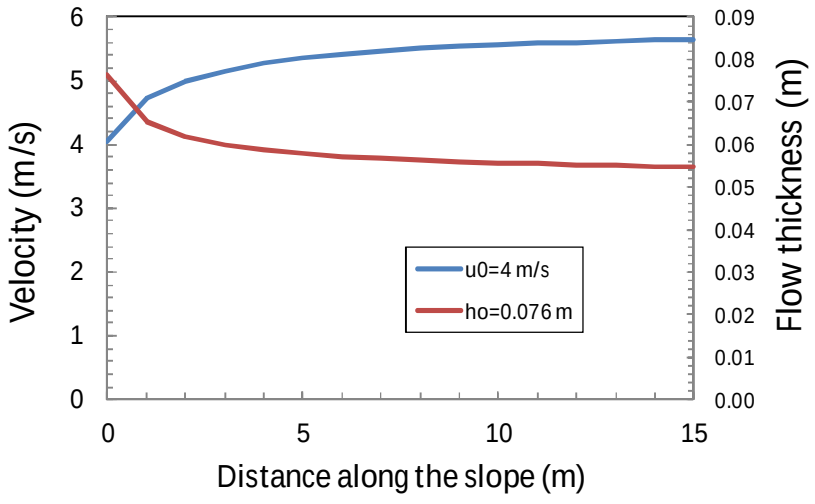

Figure 3.6 Flow velocities and thicknesses along a 1:3 slope, starting with a velocity of u_o = 4 m/s at the crest

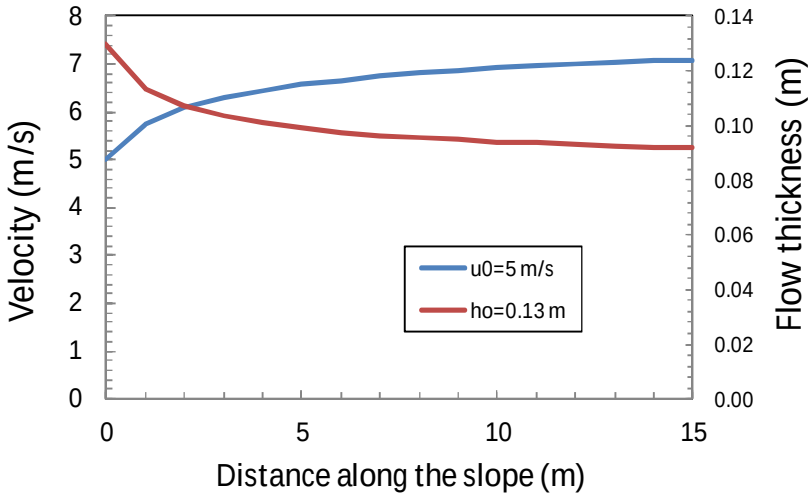

Figure 3.7 Flow velocities and thicknesses along a 1:3 slope, starting with a velocity of u_o = 5 m/s at the crest

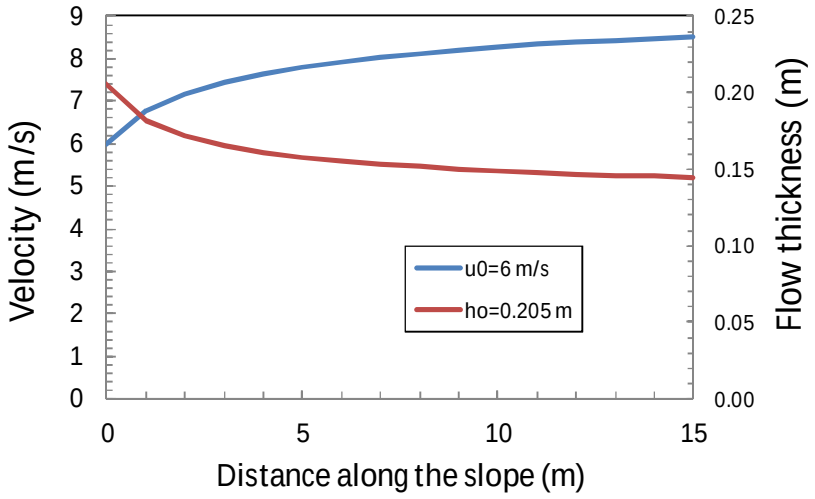

Figure 3.8 Flow velocities and thicknesses along a 1:3 slope, starting with a velocity of u_o = 6 m/s at the crest

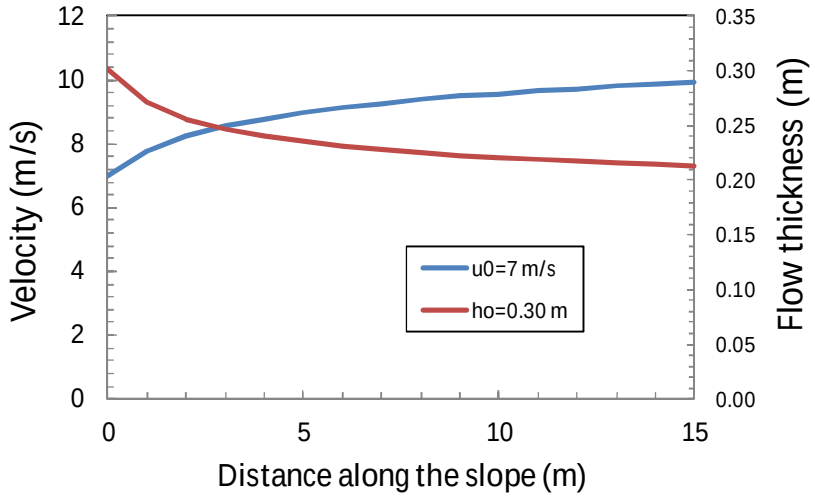

Figure 3.9 Flow velocities and thicknesses along a 1:3 slope, starting with a velocity of u_o = 7 m/s at the crest

A distance of 10 m down the slope is not so far from the transition to the toe, and in most cases the velocities have then become more or less constant (terminal velocity). Therefore a distance of 10 m along the slope has been chosen to calculate the cumulative overload again. It appears that at 10 m down the slope the velocities have increased by about 37% compared to the initial velocity at the crest (within 1% accuracy). The distribution of overtopping wave volumes for each subtest was used again, but now all velocities were increased by 37%. Then the cumulative overload of each subtest was calculated again. Due to the larger velocities more waves had to be counted which contribute to the cumulative overload. So, this cumulative overload increases due to the increase of velocity itself, but also by the increase of number of overtopping wave volumes with a velocity larger than the critical velocity.

Tables 3.3 and 3.4 are similar to Tables 3.1 and 3.2 with the only exception that the cumulative overload has now been calculated 10 m down a 1:3 slope and not at the crest. It is probably these cumulative overload values that have to be used for prediction of the behavior of the grassed slope.

q	0.1	1	5	10	30	50	75	100	150	200
	l/s per m	l/s per m	l/s per m	l/s per m	l/s per m	l/s per m	l/s per m	l/s per m	l/s per m	l/s per m
uc=4 m/s	1	7	59	173	991	2164	4367	6792	11320	15344
uc=5 m/s			4	17	195	574	1308	2157	5484	8890
uc=6.3 m/s					5	32	119	579	934	2004

Table 3.3 Cumulative overload (m^2/s^2) for various discharges and critical velocities and for a duration of 1 hour assuming H_s = 1 m). Location: 10 m down a 1:3 slope

q	1	10	50	100	200
	l/s per m	l/s per m	l/s per m	l/s per m	l/s per m
uc=4 m/s	42	1080	14064	54816	146880
uc=5 m/s		102	3546	16488	69828
uc=6 m/s		0	192	3666	15690

Table 3.4 Total cumulative overload (m^2/s^2) for a sequence of 5 subtests with various critical velocities and for a duration of 6 hours for each subtest (assuming H_s = 1 m). Location: 10 m down a 1:3 slope

3.3.3 Effect of turbulence on slope

It has been assumed in the above section that the turbulence intensity remains constant between the crest and a location somewhere along the slope. However, the turbulence intensity will decrease if the flow velocity increases and the water depth decreases. This phenomenon was shown in the evaluation report of the measurements on the Vecht dike (see section 2.1.7; SBW, 2010). In that report a relation was derived and verified between the turbulence intensity r_o and the air content ε as a function of the water depth h:

$$r_0 = 1{,}2\sqrt{\frac{{}^{1}/_{18}\, p_m}{\rho U^2}} \text{ met } p_m = 18\rho g h(1-\varepsilon)S_b \qquad (3.7)$$

As the hydraulic load on the slope is determined by the product of r_o and U the following ratio can be derived:

$$\frac{(r_0 U)_{crest}}{(r_0 U)_{slope10m}} = \frac{\left(\sqrt{h(1-\varepsilon)}\,U\right)_{crest}}{\left(\sqrt{h(1-\varepsilon)}\,U\right)_{slope10m}} \qquad (3.8)$$

The ratio enables to compare the hydraulic load at different locations along a slope. This has been elaborated for a critical flow velocity of U_c = 5 m/s as an example. From Figure 3.7 the following values can be taken:

At the crest: U = 5 m/s and h = 0.13 m
At 10 m: U = 7 m/s and h = 0.09 m

The air content can be estimated with: $\varepsilon \approx 6 + 20\sqrt{5h - 0.2}$ (see SBW, 2010) resulting in:

At the crest: $\varepsilon = 19.5\%$
At 10 m: $\varepsilon = 16\%$

Substituting all values results in a ratio of: $\frac{(r_0 U)_{crest}}{(r_0 U)_{slope10m}} = \frac{1.618}{1.925} = 0.84$

The result is a value smaller than 1 meaning that the total hydraulic load at 10 m is higher than at the crest. Consequently, erosion will occur earlier at locations on the lower part of the slope than at locations higher on the slope.

In section 3.3.2 it was shown that the cumulative overload increases for U_c = 5 m/s, q = 50 l/s per m and a duration of 6 hours from 12 m^2/s^2 (see Table 3.2) to 3550 m^2/s^2 (see Table 3.4). This increase is due to the increase of the flow velocity from 5 m/s at the crest to 7 m/s at the slope at 10 m, an increase of 37%. The combined effect of increased flow velocity and reduced turbulence results in an increase of 19% (inverse of 0.84). Thus, the cumulative overload will increase, but to a lower value than 3550 m^2/s^2.

3.4 Fast test on critical velocity

In the prediction phase one has to rely on clay and grass investigations to predict the critical velocity for the test section (= strength parameter of the slope). Maybe the testing will show when damage and failure will occur. Another way, and also a way to validate the method of cumulative overload, is to perform short tests with only large overtopping waves. In such a case overtopping wave volumes with velocities lower or close to the critical velocity are neglected and only overtopping wave volumes which may contribute to a - a priori - selected critical velocity will contribute to developing damage.

For determining the critical velocity a (special) reference strip is chosen, so it will not be influenced by other tests. Overtopping volumes larger than 1.5 m^3 per m contribute to the cumulative overload if u_c =4 m/s. The test with q = 100 l/s per m has a maximum of about 2.5 m^3 per m. It is proposed to use as a first subtests only overtopping wave volumes of 1.5, 2.0 and 2.5 m^3 per m. These three overtopping wave volumes have a total cumulative overload of 44 m^2/s^2 at the crest and 124 m^2/s^2 at 10 m down the slope, see Table 3.5. By repeating these three overtopping wave volumes the cumulative overload will increase, see Table 3.6. With 50 repeats of the three overtopping wave volumes a cumulative overload of more than 6000 m^2/s^2 at 10 m down the slope will be reached, using a critical velocity of 4 m/s. If the slope indeed fails within this test, the critical velocity will be in the order of 4 m/s. If the slope does not fail, one has to continue the test with larger overtopping wave volumes. This first test contains 150 waves and will take 3000 s with a filling discharge of 100 l/s per m, which is less than one hour.

V	$(u^2-u_c^2)$ for 4 m/s	
(l/m)	(m^2/s^2)	
	at crest	at 10 m
1500	10	32
2000	15	42
2500	19	50
	44	124

Table 3.5 Cumulative overload for 3 overtopping wave volumes

V	$\Sigma(u^2-u_c^2)$ for 4 m/s	
(l/m)	(m^2/s^2)	
	at crest	at 10 m
repeat 10x	436	1239
repeat 20x	872	2479
repeat 30x	1308	3718
repeat 40x	1744	4958
repeat 50x	2181	6197

Table 3.6 Cumulative overloads for repeating 3 overtopping wave volumes. u_c = 4 m/s

A second test with larger overtopping volumes is given in Tables 3.7 and 3.8. Cumulative overload values have now been calculated for a critical velocity of u_c = 5 m/s. The test will take 4500 s.

V	$(u^2-u_c^2)$ for 5 m/s	
(l/m)	(m^2/s^2)	
	at crest	at 10 m
2000	6	33
3000	14	48
4000	22	62
	41	143

Table 3.7 Cumulative overload for 3 overtopping wave volumes

V	$\Sigma(u^2-u_c^2)$ for 5 m/s	
(l/m)	(m^2/s^2)	
	at crest	at 10 m
repeat 10x	414	1434
repeat 20x	827	2868
repeat 30x	1241	4302
repeat 40x	1654	5736
repeat 50x	2068	7170

Table 3.8 Cumulative overloads for repeating 3 overtopping wave volumes. u_c = 5 m/s

If the slope has not failed for the two subtests described, then the critical velocity is probably larger than u_c = 5 m/s. It is than possible to continue with a third test with even larger velocities. Tables 3.9 and 3.10 give these three larger overtopping wave volumes, which include the maximum volume of 5.5 m^3 per m.

V	$(u^2-u_c^2)$ for 6.35 m/s	
(l/m)	(m^2/s^2)	
	at crest	at 10 m
4000	7	48
5000	13	60
5500	17	66
	37	174

Table 3.9 Cumulative overload for 3 overtopping wave volumes

V	$\Sigma(u^2-u_c^2)$ for 6.3 m/s	
(l/m)	(m^2/s^2)	
	at crest	at 10 m
repeat 10x	370	1738
repeat 20x	739	3476
repeat 30x	1109	5213
repeat 40x	1478	6951
repeat 50x	1848	8689

Table 3.10 Cumulative overloads for repeating 3 overtopping wave volumes. u_c = 6.3 m/s

The duration of this subtest with a filling discharge of 100 l/s per m will be 7500 s, just a little more than 2 hours.

All three subtests together come to a total overtopping duration of about 4 hours, which makes it possible to perform these three tests in one working day. It should be noted that Tables 3.7 – 3.10 are based on the given subtest only. In reality one has also to calculate the cumulative damage of the previous subtest, for the correct critical velocity. This will be taken into account for the analysis that will be performed after the tests.

4 Sod openness and root density

4.1 Introduction and sampling locations

Wave overtopping experiments will be carried out on primary dikes along the river Waal, near Nijmegen and Millingen aan de Rijn, in January and February 2013. A prediction model is to be run in advance in order to predict the strength of the dike grassland in relation to the wave overtopping tests. To provide input data for the predictive modelling, Alterra carried out fieldwork on the intended wave overtopping test locations.

The fieldwork was carried out on 2 and 3 October 2012 and aimed at collecting data on the actual dike grassland quality. The fieldwork combined methods prescribed for the third Dutch dike assessment (V&W, 2007) and newly developed field methods for the prolonged third assessment round (ENW, 2012). In total, five plots were sampled on two different locations. Location 1 was less than 100 metres northeast of the 'Hollands-Duits gemaal' pumping station near Nijmegen. Location 5 was situated just west of the town of Millingen aan de Rijn (Figure 4.1) (see also Chapter 2 for a more detailed description of the locations).

Table 4.1 describes the characteristics of the wave overtopping test strips. We sampled immediately next to the intended test strips. Figures 4.2 and 4.3 show the locations of the sampled plots.

Figure 4.1 Situation of the two locations for the wave overtopping tests

Location name	Location no.	Characteristic of wave overtopping test strip	Corresponding sampled plot (bordering the test strip)
'Hollands-Duits gemaal' pumping station, Nijmegen	1	No object on test strip	Hollands-Duits gemaal 1
	1	Concrete cap blocking lower side of test strip	Hollands-Duits gemaal 2
	1	Concrete cap reaching halfway into lower side of test strip	Hollands-Duits gemaal 3
Millingen aan de Rijn	5	Damaged verge immediately bordering asphalt road on crest, outer slope side	Millingen outer slope
	5	Damaged verge immediately bordering asphalt road on crest, inner slope side	Millingen inner slope

Table 4.1 Characteristics of wave overtopping test strips and corresponding labels

The measurements were concentrated on the visually weakest spots immediately next to the intended wave overtopping test strips. At Location 5 (near Millingen aan de Rijn) the two verges directly next to the asphalt road were hardly covered by grass or herbs. The bare underground consisted partly of asphalt, partly of brick debris, slack and sand. It proved impossible to sample these 'stony' verges for root density.

Figure 4.2 Situation of the sampled plots on Location 1, just east of Nijmegen. Each red dot represents a sampling plot that immediately borders the intended wave overtopping test strip and runs parallel to it on the dike slope

Figure 4.3 Situation of the sampled plots on location 5, west of Millingen aan de Rijn. Each red dot represents a sampling plot that immediately borders the intended wave overtopping test strip and runs parallel to it on the dike slope

4.2 Methodology

Measurements focused on sod openness on the one hand and root density on the other. For both variables, methods prescribed for the third assessment round (V&W, 2007) and newly developed methods proposed for the prolonged third assessment round (ENW, 2012) were applied alongside.

4.2.1 Measurements according to third assessment round

The methods prescribed for the third assessment round are described in detail in Appendix 8-1 of the Dutch Safety Assessment Regulation (V&W, 2007). The applied methods for establishing root density and sod cover are briefly described below.

Root density

The Dutch Safety Assessment Regulation prescribes that root density has to be estimated by the so-called ‘hand method’. A gouge auger is used to sample the top 20 cm of the grass sod,

which is divided into eight layers of 2.5 cm thickness. In each layer, the number of root fragments of > 1 cm length is estimated as a measure of root density. Based on this count, the quality of the sod root density is expressed in four categories: ‘very poor’, ‘poor’, ‘moderate’ and ‘good’.

We extended our measurements to a depth of 50 cm. This was done because previous work at other locations showed that a significant amount of roots may be present at depths greater than 20 cm. Sampling to 50 cm depth was considered relevant in particular for the intended wave overtopping tests which might be carried out at the same locations some other time.

Sod cover (grid method)
The Dutch Safety Assessment Regulation (V&W, 2007) mentions aboveground plant (shoot) cover as a quality indicator for dike grass sods (next to species composition, which is related to management type). A cover value of 70% is presented as a threshold value separating different quality classes. The Safety Assessment Regulation does not prescribe by what method shoot cover should be measured. It may be estimated visually, but in order to ensure standardised measurements we used a grid in a 50 x 50 cm frame with 81 measuring points. Where necessary for easier measurement, the vegetation is cut back to a height of about 2 cm[1]. When estimating plant cover, no distinction is made between grasses and other herbaceous plants or forbs. However, mosses are not taken into account in the measurement as they have no proper roots and do not contribute to the strength of the sod. For every grid intersection (measuring point) a long needle is pricked perpendicularly into the sod, and it is determined whether there is 'plant contact' or 'ground contact'. The number of measuring points with 'plant contact', relative to the total number of measurement points, is a measure of the percentage sod cover[1]. In each sample plot, sod cover was measured on three visually weak spots. Afterwards, the percentage cover for the three separate measurements were averaged for the sample plot.

4.2.2 Measurements according to prolonged third assessment round

Anticipating the prolonged third assessment round, a new method for estimating grass sod quality was proposed in section 6.4.2 of ENW (2012). The newly proposed method consists of a visual inspection of the sod openness, and an estimation of the sod strength (related to root density) by means of the so-called ‘spade method’. It is advised that the visual inspection be carried out in all instances. It is recommended that the spade method is carried out only in case of doubt about the sod quality as estimated by the visual inspection (ENW, 2012). We applied the spade method at every sample plot, with one measurement at the visually weakest spot.

Sod cover (visual estimation of openness)
Based on visual inspection (ENW, 2012) the grass sod can be divided into one of three categories: closed, open or fragmentary sod. The visual inspection has to be done within a 5 x 5 m square area. The new visual inspection method differs from the grid method (V&W, 2007) in that it explicitly demands to look for the presence of greater open spots and their potential presence has consequences for the quality verdict.

Root density, spade method
In case of doubt about the sod cover quality verdict as estimated by the visual inspection, a grass sod of 25 x 30 cm, with a thickness of about 7 cm, is to be cut loose using a spade. The

[1] *Cutting back of the shoots implies that the percentage shoot density rather than the percentage shoot cover is estimated by the grid method.*

sod strength (or root density) is divided into one of three categories: high root density, moderate root density or fragmentary root density (ENW, 2012). According to the prescription, the spade method has to be done on a representative spot within a homogeneously looking part of the slope. For the purpose of the current study, we applied the spade method on all sampled plots and carried out one measurement on the visually weakest spot.

4.3 Results

Table 4.2 gives a description of the sod appearance as well as the percentage sod cover and quality verdicts for sod cover and root density as determined by the different methods applied. According to the method of the third assessment round (V&W, 2007), the sod cover for all plots near Nijmegen ('Hollands-Duits gemaal') is well below 70% (poor). The sod cover for all plots near Millingen aan de Rijn is well above 70% (good). According to the method of the prolonged third assessment round, the sod cover for all plots near Nijmegen is categorized as open and the plots near Millingen are categorized as closed.

Sample plot	Sod description	Sod cover		Root density	
		V&W (2007)	ENW (2012)	V&W (2007)	spade method (ENW, 2012)
Hollands-Duits gemaal 1, no object on test strip	open sod, large amount of mown litter	60% (poor)	open	very poor	moderate
Hollands-Duits gemaal 2, concrete cap blocking lower side of test strip	open, bumpy sod with tussocks	53% (poor)	open	poor	fragmentary
Hollands-Duits gemaal 3, concrete cap reaching halfway into lower side of test strip	open sod, damaged by tractor	46% (poor)	open	poor	high
Millingen outer slope	closed sod, not mown	91% (good)	closed	moderate	high
Millingen inner slope	high and rough vegetation, not mown	88% (good)	closed	moderate	high

Table 4.2 Sod cover and root density for the third (V&W, 2007) and prolonged third (ENW, 2012) assessment rounds. The quality verdict for root density according to V&W (2007) can be read from the graphs displayed in the Appendix

4.4 Concluding remarks

The outcomes of both methods (V&W, 2007 and ENW, 2012) correlated very well for sod cover and showed that the vegetation at Location 5 (near Millingen aan de Rijn) was more closed than at Location 1 (near Nijmegen).

The quality verdict based on root density mostly gave higher root densities for Location 5 than for Location 1, but otherwise showed contrasting results for the two methods. The difference between the outcomes may reflect small-scale differences in root density, as the two methods cannot be applied to exactly the same spot. In all cases, sampling focused on visually weak spots, but sample sizes differed with n = 1 for the spade method and n = 3 for the gouge auger method, It is planned to repeat the root density measurements on all sample plots early

in 2013, coinciding with the wave overtopping tests. Both root density methods will then be applied again but with increased sample size for the spade method.

In conclusion, the dike grassland at Location 1 near Nijmegen is expected to be weaker and more prone to failure during wave overtopping events than the dike grassland at Location 5 near Millingen aan de Rijn. However, as it was not possible to determine root density on the bare road shoulders on Location 5 (due to the very stony underground), it may be that this location is actually quite vulnerable to damage or failure due to wave overtopping, as the transition from asphalt road to bare shoulder and closed grass sod may well be very weak, as is known from previous wave overtopping tests at Tholen (2011). The two root density methods will be repeated with equal sample sizes on the same locations early in 2013. This will allow to better understand the relationship between the outcomes of the two methods.

4.5 References

ENW. 2012. Technisch Rapport Toetsen Grasbekledingen op Dijken. Version 1 (final), 9 May 2012.

V&W, 2007. Dutch Safety Assessment Regulation (Voorschrift Toetsen op Veiligheid voor de derde toetsronde 2006 – 2011). Ministry of Transport and Infrastructure (V&W). URL: http://www.helpdeskwater.nl/publish/pages/5259/vtv2006.pdf.

5 Grass modelling

5.1 Introduction

This Chapter describes the prediction of the critical depth-averaged flow velocity (U_c) for grass covers at two locations i.e. in Millingen and near the Hollands-Duits pumping station in Nijmegen. This prediction is based on root tensile-stress tests (root properties; lower boundary) and grass sod tensile-stress tests (soil properties; upper boundary).

Alterra (Paulissen 2010) carried out more than 500 laboratory tests in which $\sigma_{root,c}$ (= critical mean root tensile-stress) and d_r (= mean root diameter) of Dutch grasses were investigated yielding $\sigma_{root,c} \approx 15 \cdot 10^6$ N/m^2 (Fig. 5.1) and d_r = 0.1 mm (standard deviation is 0.05 mm). It is recommended to summarize these experimental results into a factual report (see also section 5.6).

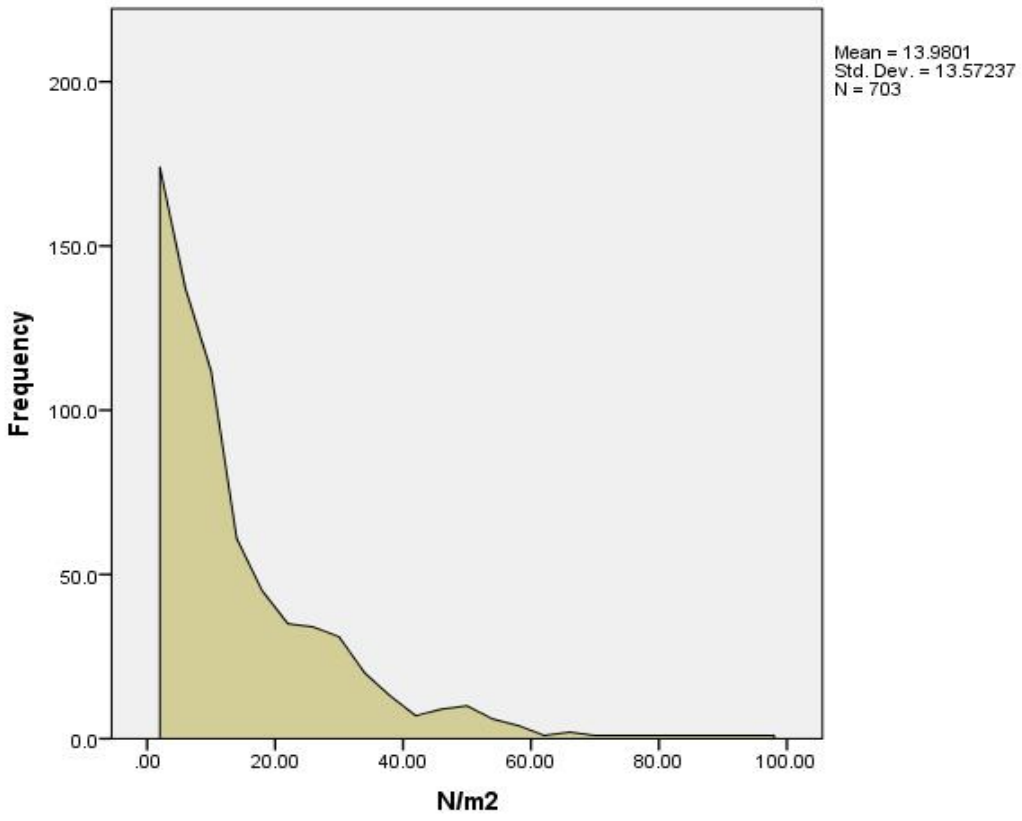

Figure 5.1 Frequency as function of the root tensile-stress (Paulissen 2010)

Recently Infram (Bakker 2012) investigated the critical lift force of grass sods with a cross-sectional area of 15 cm x 15 cm = 225 cm^2 and a thickness of about 5 cm (range is 3 cm to 6 cm for the considered tests) at different locations for both unsaturated soil conditions and conditions where the larger pores/cracks were saturated (Fig. 5.2). Moreover, two different force transmissions were tested, where either two or four sides of the tested piece of sod were cut:

1) Force transmission through the underside of the grass sod only (Condition A);
2) Force transmission through the underside and two sidewalls (Condition B).

Figure 5.2 Grass sod tensile-stress apparatus

The force transmission of the local bed pressure fluctuations caused by overtopping waves goes through the four sidewalls and the underside of grass sods. Assuming that the strength of grass is obtained by the roots only (thus the influence of suction pressures in the clay aggregates is neglected) the critical mean lift force of the grass sod with dimensions of 15 cm x 15 cm x 5 cm varies from 0.05 kN to 0.2 kN (Table 5.1). In the next two sub-sections, this range is discussed in relation to measured forces.

Quality of grass (VTV-2006)	**No. of roots (VTV-2006)**	**No. of roots (15 cm x 15 cm)**	**Critical mean lift force (15 cm x 15 cm) [kN]**
Very poor	< 18	< 600	< 0.07
Poor	18 – 32	600 – 1000	0.07 – 0.12
Averaged	32 – 45	1000 – 1400	0.12 – 0.17
Good	> 45	> 1400	> 0.17
Critical mean lift force: $F_{l,c}$ = No. (15 cm x 15 cm) · A_{root} · $\sigma_{root,c}$ with $A_{root} = \frac{1}{4} \pi (d_r)^2$ where $\sigma_{root,c} = 15 \cdot 10^6$ N/m^2 and d_r = 0.1 mm			

Table 5.1 Properties of Dutch grasses

5.2 Millingen

When the bottom of the grass sod contributes in the force transmission only, experiments at Millingen showed (Table 5.2a) that the critical lift force varied from 0.43 kN (when the larger pores were saturated) to 0.56 kN (for unsaturated conditions). When the side walls also contributed the critical lift force increased and ranged from 0.90 kN (when the large pores were saturated) to 0.99 kN (for unsaturated soil conditions) (Table 5.2b).

No side walls				2 side Walls			
	Critical Lift force	Mean value	Thickness(1) Grass sod		Critical Lift force	Mean Value	Thickness(1) Grass sod
Test	[kN]	[kN]	[cm]	Test	[kN]	[kN]	[cm]
1D4.1	0.50		4.5	1D2.1	0.88		4.0
1D4.2	0.61	0.56	-	1D2.2	1.09	0.99	-
1N4.1	0.48		3.5	1N2.1	0.92		4.0
1N4.2	0.38	0.43	3.0	1N2.2	0.88	0.90	4.0
(1) In the calculations the thickness of the grass sods is assumed 5 cm.							

Table 5.2 a Experimental results (Millingen) b Experimental results (Millingen)

Next, the normal grass stresses (acting on the bottom of a grass sod) and the shear grass stresses (acting on the sidewalls) are discussed. Subsequently, the static force balance is used to estimate the root strength.

Usually, the root intensity is at maximum near the soil surface and decreases exponential with the depth. Therefore, the critical mean normal grass stress at 5 cm beneath the surface can be approximated by (Figs 5.3 and 5.4, see also Appendix C)

$$\sigma_{grass,c}(-0.05/\lambda_{ref}) = \sigma_{grass,c}(0)\exp(-0.5) = 0.6\sigma_{grass,c}(0)$$

in which λ_{ref} (= 0.10 m) is a reference height. The critical mean shear grass stress at the sidewalls is (see also Appendix F)

Figure 5.3 Detail of grass sod tensile stress apparatus

Figure 5.4 Detail of grass sod tensile-stress apparatus (thickness of the grass sod is about 5 cm)

$$\tau_{grass,c} = \frac{1}{0.05}\int_{-0.05}^{0} \sigma_{grass,c}\left(z/\lambda_{ref}\right)\mathrm{d}z$$

or

$$\tau_{grass,c} = \frac{1}{0.05}\int_{-0.05}^{0} \sigma_{grass,c}(0)\exp\left(z/\lambda_{ref}\right)\mathrm{d}z$$

or

$$\tau_{grass,c} = 0.8\sigma_{grass,c}(0)$$

The critical downward force reads (for two sidewalls)

$$F_{d,c} = 2F_{s,c} + F_{b,c}$$

where the contributions of the sidewalls ($F_{s,c}$) and the bottom ($F_{b,c}$) are

$$F_{s,c} = \tau_{grass,c} \cdot A_s$$

$$F_{b,c} = 0.6\sigma_{grass,c}(0) \cdot A_b$$

Considering static equilibrium conditions thus the critical lift force equals the critical downward force ($F_{\ell,c} = F_{d,c}$) and assuming that the suction pressures are negligible, $\sigma_{grass,c}(0)$ is for soil in which cracks are saturated (pores in clay aggregates are unsaturated)

Condition A (no side walls)

$$F_{\ell,c} = F_{d,c} = F_{b,c} = 0.6\sigma_{grass,c}(0) \cdot A_b$$

or

$$\sigma_{grass,c}(0) = \frac{F_{\ell,c}}{0.6A_b} = \frac{0.43}{0.6 \cdot 0.15 \cdot 0.15} = 31.9 \text{ kN/m}^2$$

Condition B (with two side walls)

$$F_{\ell,c} = 2F_{s,c} + F_{b,c} = 2\tau_{grass,c} \cdot A_s + 0.6\sigma_{grass,c}(0) \cdot A_b = \sigma_{grass,c}(0)(2 \cdot 0.8A_s + 0.6A_b)$$

or

$$\sigma_{grass,c}(0) = \frac{F_{l,c}}{0.6A_b + 2 \cdot 0.8A_s} = \frac{0.90}{0.6 \cdot 0.15 \cdot 0.15 + 2 \cdot 0.8 \cdot 0.15 \cdot 0.05} = 35.3 \text{ kN/m}^2$$

Hence, $\sigma_{grass,c}(0)$ is nearly independent of the type of force transmission. Moreover, $\sigma_{grass,c}(0)$ is 4 to 5 times greater than the value based on root properties only (see also Appendix C where $\sigma_{grass,c}(0)$ = 7.5 kN/m^2 for good grass). Since the experiments were carried out during sunny conditions (on Thursday 23 August 2012) most likely suction pressures have influenced the experimental results significantly.

The high tensile stresses obtained from the apparatus as shown in Figure 5.1 are based on static equilibrium conditions; no dynamic forces were considered. Probably the grass cover on the dike fails due to fatigue. If this hypothesis is true then the critical lift force (Table 5.2) should be less analogous to the fatigue strength of steel, concrete and other civil materials. Since the measurements do not support the “state of the art” models more research is recommended.

The maximum lift force acting on the grass sod can be given by

$$F_\ell = p_m A_b = 2.25 \cdot 10^{-2} p_m$$

where p_m represents the maximum pressure fluctuation near the bed. By using the turf element model it follows that (Appendix D)

$$F_{\ell,c} = 4A_s\tau_{grass,c} + A_b \cdot 0.6\sigma_{grass,c}(0)$$

or

$$F_{\ell,c} = 4A_s \cdot 0.8\sigma_{grass,c}(0) + A_b \cdot 0.6\sigma_{grass,c}(0)$$

or

$$F_{\ell,c} = 4 \cdot (0.15 \cdot 0.05) \cdot 0.8 \sigma_{grass,c}(0) + (0.15 \cdot 0.15) \cdot 0.6 \sigma_{grass,c}(0)$$

or with (Emmerling 1973)

$$p_{m,c} = 18 \tau_c$$

the critical bed shear stress can be given by

$$18 \tau_c = 1.67 \sigma_{grass,c}(0)$$

or with 31.9 kN/m^2 < $\sigma_{grass,c}(0)$ < 35.3 kN/m^2 the critical bed shear stress is

$$3.0 < \tau_c = 0.093 \sigma_{grass,c}(0) < 3.3 \text{ kN/m}^2$$

Note that this value of τ_c is extremely high (Table 5.3). By applying (Hoffmans 2012)

$$\tau_c = \rho \frac{g U_c^2}{C^2} = 0.7 \rho (r_0 U_c)^2 \quad \text{with} \quad r_0 = 1.2 \frac{\sqrt{g}}{C}$$

Suction pressure

Clay shrinks and expands as a result of drying and wetting, and these changes are directly connected to changes in the water content of the clay. Above the water table the pore water pressure in clay is usually negative in relation to the atmospheric pressure. This under (or negative) pore water pressure is usually referred to as suction pressure because clay can 'suck up' water from the water table. The suction pressure holds the water films around the aggregates. As more water drains, the films of water around the aggregates become thinner and the air-water interface becomes sharply curved, leading to increased suction.

The pore water pressure in the larger pores only becomes positive when water percolates directly through these open spaces due to precipitation or infiltration by outside water. However, in the smaller pores of the aggregates into which water cannot easily infiltrate there are still underpressures. As a result of the water overpressures the water in the larger pores is attracted to the water in the smaller aggregates. Consequently, the aggregates gradually swell. This time-dependent process of volume change is slow because of the low permeability of the aggregates.

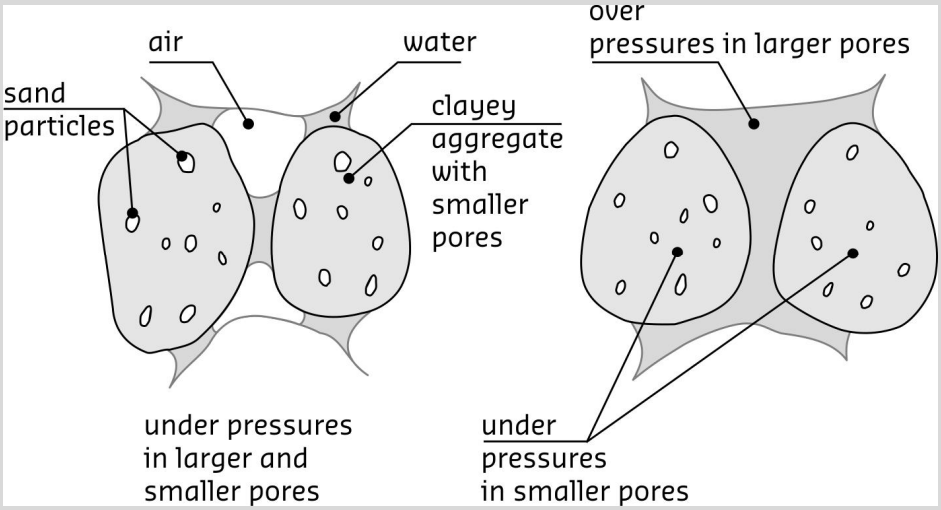

Clayey aggregates before and after infiltration

Evaporation into the atmosphere also plays an important role in the suction pressure, and this can take place directly from the soil into the atmosphere or via the vegetation. Among other factors, the rate of evaporation is dependent on the relative humidity of the air. Close to the surface of a dike, the suction pressure can be often higher than 1000 kN/m^2 (or a 100 m head of water) in the summer, mainly as a result of the relatively high temperature and the suction power of the vegetation. Precipitation and temperature changes can allow this suction pressure to vary greatly and when it rains, it is often less than 50 kN/m^2.

In winter conditions, in wet periods, on average the suction pressure in the clay cover of a dike is usually less than 10 kN/m^2. The suction pressure can be considerably higher only in dry freezing air, especially in south facing banks. The greatest changes in suction pressure take place in the turf layer due to changes in precipitation, water extraction by roots, and very large temperature differences. Variations in the suction pressure in the core of the dike are caused by changes in the position of the water table, and by atmospheric effects. The effects of changes in atmospheric conditions are very slight and the variations in suction pressure in the dike core are usually slow and of limited size.

The suction pressure in the core of a dike can vary from 0 kN/m^2 to rarely more than 50 kN/m^2. According to Ingles (1962) the suction pressure is inversely proportional to the particle diameter or to the dimensions of the capillaries, thus the suction pressure increases with a decreasing hydraulic conductivity. The suction pressure also depends on how much water is in the soil. If the soil is completely saturated the suction pressure is nil. The figure as shown below presents the suction pressure (through the pF curve) as function of the water content.

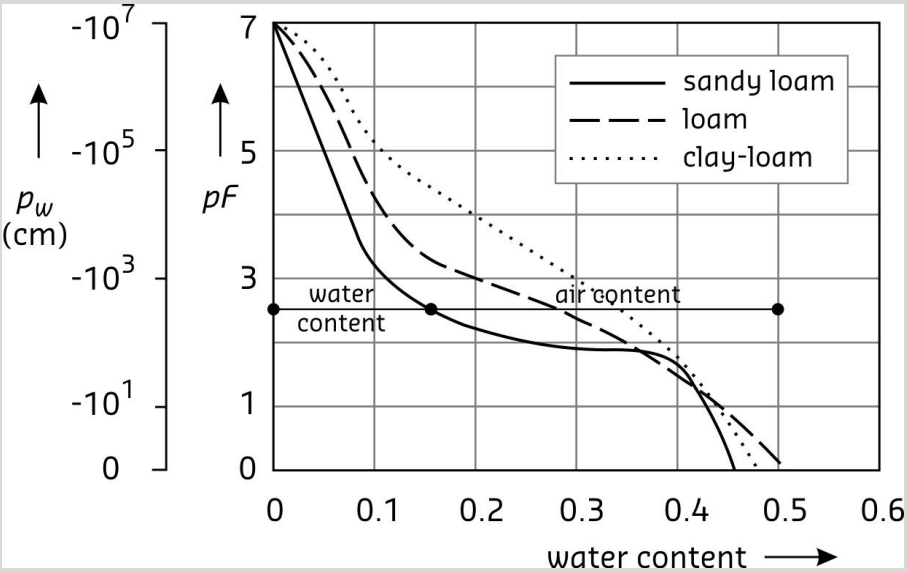

Suction pressure as function of water content

where C is the Cheesy coefficient, r_0 represents the relative depth-averaged turbulence intensity and ρ is the density of the water, the critical depth-averaged flow velocity is.

$$U_c = \frac{1}{r_0}\sqrt{\frac{\tau_c}{0.7\rho}} = \frac{1}{0.12}\sqrt{\frac{3100}{700}} = 17{,}5\ \mathrm{m/s}$$

Note that r_0 depends on the flow velocity, flow depth and the steepness of the dike slope. For a first approximation r_0 is here assumed to be $r_0 = 0.12$. Most likely the calculated U_c is too high (see also Table 5.3). There are two reasons for this result.

In the grass sod tensile-stress tests the deformations were not reported. Probably the critical deformations corresponding to the critical tensile forces are too large, say a few centimetres. When the erodibility of grass is tested under prototype conditions the deformations lie in the range of 1 mm to 1 cm. Therefore, it is recommended to measure the relation between deformations and forces in the next tests.

Furthermore, it is recommended to study the effects of fatigue, which is here not considered. Note that the critical force decreases when the number of waves increases. Finally, it is also recommended to investigate the influence of the root intensity as function of the depth. According to the VTV-2006 the distribution is exponential. However, the latest insights show that the root-intensity at larger depth is linear.

Soil		τ_c	U_c
		(N/m^2)	(m/s)
Grass (1)	good	125 – 250	5.0 – 8.0
	average	50 – 125	3.0 – 5.0
	poor	25 – 75	2.0 – 4.0
	very poor	5 – 25	1.0 – 2.0
Clay (2)	good	1.5 – 5.0	0.7 – 1.0
	average/structured	0.5 – 1.5	0.5 – 0.7
	poor	0.3 – 0.5	0.3 – 0.5
Sand		0.1 – 0.2	0.15 – 0.3

(1) Quality of grass is mainly determined by the root intensity and apparent cohesion; quality of clay is of second importance.
(2) Without roots

Table 5.3 Indicative values of τ_c and U_c for different types of soil (Verheij et al. 1995)

The Vechtdijk, a Dutch dike along the river Vecht, consists of about 90% sand. The erodibility of the grass cover was tested during the winter season 2010 when roots usually are at their weakest strength. However, the root investigation showed that the number of roots and the cover ratio were still qualified as “good”. During the experiments the sand in the top soil was cemented giving the turf aggregate sufficient strength for compression which is required since the load of overtopping waves generates over pressures as well as under pressures. Note that the under pressures dominate the erosion process.

Because of the relatively high permeability of sand, the infiltrated water resulting from overtopping waves reduces the suction pressure almost at once in both the larger and smaller pores. Therefore, after infiltration the apparent cohesion is probably negligible in and under the turf layer. On the sandy Vechtdijk, experiments in which the significant wave height varied (H_s = 1 m, 2 m and 3 m) showed that the critical depth-averaged flow velocity is about $U_c \approx 4$ m/s (see also Table F1 in Appendix F)

According to Van Adrichem (2012), the grass quality at Millingen is moderate (grass on a clayey dike). Following Schaffers et al. (2011), seasonal variations between winter time (before 1 March) and early October can be neglected. Assuming that the grass quality will also be moderate during the wave overtopping tests and neglecting the influence of suction pressures the critical depth-averaged flow velocity is approximately 4 m/s (see also Table F1 in Appendix F). Including the effects of suction pressures U_c may vary from 6 m/s to 7 m/s depending on the magnitude of the suction pressures.

Summarizing, two different grass revetments can be distinguished, namely a grass revetment on a sandy dike (sand contents is greater than 90%) in which the sand is cemented (Vecht-dijk) and a grass revetment that consists of roots and clay. In the modelling, the erodibility of grass is determined by the root intensity and the suction pressures. For sandy dikes the suction pressures are negligible after infiltration. However, for a clayey cover there is still apparent cohesion in the smaller clay aggregates, thus roots in clay are stronger than roots in cemented sand.

During winter conditions, the suction pressures (p_w) lies in the range of – 5 kN/m^2 to – 10 kN/m^2 (Van Ooijen 1996). If the following assumptions are made p_w = – 7.5 kN/m^2 and the

root intensity satisfies the grass quality 'moderate' then $\sigma_{grass,c}(0)$ (= 6 kN/m^2, see Appendix C Table C2); and U_c are

$$\sigma_{grass,c}(0) - p_w = 7.5 + 6.0 = 13.5 \text{ kN/m}^2$$

and

$$U_c = \frac{1}{0.12}\sqrt{\frac{0.093 \cdot 13500}{700}} = 11.2 \text{ m/s}$$

resulting in a too high value of U_c.

As the friction factor is related to the Chezy by (see also SBW report 2012 Model Development).

$$C = \sqrt{\frac{2g}{f}}$$

and C to r_0

$$C = 1.2\frac{\sqrt{g}}{r_0}$$

f can be expressed by

$$r_0 = 0.85\sqrt{f}$$

The friction factor may vary from 0.01 to 0.1 (SBW report 2010 Model Development). Hence, r_0 ranges from 0.08 to 0.27. Assuming that r_0 = 0.2, in stead of 0.12 used previously (Hoffmans 2012, Section 5), the critical depth-averaged flow velocity becomes about 7 m/s in stead of 11.2 m/s. Hence, the grass slope itself will not fail during the wave overtopping discharge q = 200 ℓ/s per unit width, however, the transition between slope and horizontal will fail within the 200 ℓ/s per unit width test (see also Table 5.5).

5.3 Hollands-Duits Gemaal

At the location of the Hollands-Duits gemaal the critical lift force measured 0.43 kN (cracks were saturated; underside and 2 side walls contributed to the force transmission; see also Table 5.4). Hence, $\sigma_{grass,c}(0)$ and U_c are (Condition B)

$$\sigma_{grass,c}(0) - p_w = \frac{F_{l,c}}{0.6A_b + 2 \cdot 0.8A_s} = \frac{0.43}{0.6 \cdot 0.15 \cdot 0.15 + 2 \cdot 0.8 \cdot 0.15 \cdot 0.05} = 16.9 \text{ kN/m}^2$$

and

$$U_c = \frac{1}{0.2}\sqrt{\frac{0.093 \cdot 16900}{700}} = 7.5 \text{ m/s}$$

According to Alterra the root intensity satisfies the grass quality poor. If the following assumptions are made p_w = – 7.5 kN/m^2 and the grass quality is poor then $\sigma_{grass,c}(0)$ and U_c are (see also Appendix C)

$$\sigma_{grass,c}(0) - p_w = 3 + 7.5 = 10.5 \text{ kN/m}^2$$

and

$$U_c = \frac{1}{0.12}\sqrt{\frac{0.093 \cdot 10500}{700}} = 9.8 \text{ m/s}$$

again this value of U_c is too high. Assuming that $r_0 = 0.2$ it follows that $U_c = 6$ m/s so the slope will fail at the start of the $q = 200$ ℓ/s per unit width (see also Table 5.5).

No side walls				2 side Walls			
	Critical Lift force	Mean value	Thickness[2] Grass sod		Critical Lift force	Mean Value	Thickness Grass sod
Test	[kN]	[kN]	[cm]	Test	[kN]	[kN]	[cm]
2D4.1	-		-	2D2.1	0.46		3
2D4.2	0.34	0.34	3	2D2.2	0.69	0.57	3
2N4.1	0.50		4	2N2.1	0.46		4
2N4.2	-	0.50[1]	-	2N2.2	0.40	0.43	4.5

[1] This value is not considered in the analysis
[2] In the calculations the thickness of the grass sods is assumed 5 cm.

Table 5.4 a Experimental results (Nijmegen) b Experimental results (Nijmegen)

5.4 Transitions and obstacles

At present, less information is available to predict the erodibility of grass near transitions and obstacles. Recently, Deltares and Van der Meer (Appendix A) proposed to extend the overload method by

$$\sum_{i=1}^{N}\left(\alpha_M U_i^2 - U_c^2\right) = D$$

where α_M is an amplification factor. For relative thick obstacles or large trees and transitions of slopes to horizontal berms α_M lies in the range of 1.0 to 1.5 (mean value is 1.25). Since there is no conceptual model to predict α_M for transitions from grass to concrete here a first approximation is given for the Hollands Duits gemaal: α_M = 1.25.

Appendix A provides insight in the prediction of α_M for both obstacles (trees, piles on the slope) and the transition of the dike slope to horizontal berm. Simple expressions for α_M are deduced. For a tree with a diameter of 1 m holds (K_{shape} = 1)

$$\alpha_M = 1.2K_{shape} = 1.2 \cdot 1.0 = 1.2$$

If the form is rectangular (for example for a vertical plate) then the shape factor measures K_{shape} = 1.2. Hence,

$$\alpha_M = 1.2K_{shape} = 1.2 \cdot 1.2 = 1.44$$

Considering a slope with a steepness of 1V:1.4H ($\beta = 35^o$) the amplification factor is

$$\alpha_M = 2\sqrt{\sin\beta} = 2\sqrt{\sin 35^o} = 1.5$$

When the slope steepness is 1V:2.7H (or $\beta = 20^o$) yields

$$\alpha_M = 2\sqrt{\sin\beta} = 2\sqrt{\sin 20^o} = 1.2$$

Table 5.4 shows computational results of the damage number as function of the overtopping discharges and the critical flow velocity.

Table 5.4 Predictions of the Damage number D (overload method); overtopping discharge varies from 1 to 150 ℓ/s per m; amplification factor ranges from 1.0 to 1.5; three value of U_c are selected U_c = 4, 5 and 6.3 m/s

α_M = 1,0							
q (ℓ/s per m)	1	10	30	50	75	100	150
U_c = 4 m/s	0	10	212	760	2011	3885	9252
U_c = 5 m/s	0	0	0	13	82	254	1081
U_c = 6,3 m/s	0	0	0	0	0	0	0
α_M = 1,1							
q (ℓ/s per m)	1	10	30	50	75	100	150
U_c = 4 m/s	0	30	425	1366	3327	6073	14084
U_c = 5 m/s	0	0	4	52	232	615	2206
U_c = 6,3 m/s	0	0	0	0	0	0	18
α_M = 1,2							
q (ℓ/s per m)	1	10	30	50	75	100	150
U_c = 4 m/s	0	67	742	2192	5002	8728	21020
U_c = 5 m/s	0	0	22	139	512	1224	3867
U_c = 6,3 m/s	0	0	0	0	0	5	83
α_M = 1,3							
q (ℓ/s per m)	1	10	30	50	75	100	150
U_c = 4 m/s	2	125	1175	3241	7011	11795	27955
U_c = 5 m/s	0	0	60	295	960	2128	6089
U_c = 6,3 m/s	0	0	0	0	3	30	240
α_M = 1,4							
q (ℓ/s per m)	1	10	30	50	75	100	150
U_c = 4 m/s	4	209	1727	4504	9325	15749	34891
U_c = 5 m/s	0	2	128	543	1610	3358	8862
U_c = 6,3 m/s	0	0	0	0	20	93	564
α_M = 1,5							
q (ℓ/s per m)	1	10	30	50	75	100	150
U_c = 4 m/s	8	322	2400	5969	11909	21002	41827
U_c = 5 m/s	0	8	237	901	2481	4923	12154
U_c = 6,3 m/s	0	0	0	6	62	219	1058

5.5 Summary

The grass erosion prediction for the different test sections is given in Table 5.5. The predictions are based on the loading supplied by the wave overtopping simulator, consisting of a string of overtopping volumes based on the theory given in section 3.1 for each simulated storm. The simulated loading is a sequence of storms: 6 hours 1 l/s per m, 6 hours 10 l/s per m, 6 hours 50 l/s per m, 6 hours 100 l/s per m and 6 hours 200 l/s per m based on H_s=1 m.

The theory of acceleration of the flow velocity on the slope (section 3) is applied. The applied acceleration multiplier on U is 1,25 (+25%). This value is in between the actual predicted flow velocity increase given in section 3.1 and 3.2 (37%) and the note of a reduction of turbulence giving an actual loading increase of 19% (section 3.3.3).

The critical flow velocity was established During winter conditions the predictions of the critical depth-averaged flow velocity of grass are 7 m/s at the river dike in Millingen and 6 m/s at the Hollands-Duits gemaal in Nijmegen. Table 5.5 gives the time during the testing where the overload reaches a value of 1000 m^2/s^2 (multiple damaged spots) and 3500 m^2/s^2 (failure of the grass cover).

Location	**Specifics**	**Overload 1000 m^2/s^2**	**Overload 3500 m^2/s^2**	**Remarks**
Nijmegen U_c=6 m/s	Slope test section 1 and 2	Just after start of 200 l/s/m test	2 hours into 200 l/s/m test	α = 1
	Transition 1:2 to horizontal (test section 1)	Just after start of 100 l/s/m test	2 hours into 100 l/s/m test	α = 1,33
	Transition 1:3 to horizontal (test section 2)	3 hours into 100 l/s/m test	1 hour into 200 l/s/m test	α = 1,12
	Transition 1:3 to vertical wall (test section 2)	4 hours into 50 l/s/m test	2 hours into 100 l/s/m test	α = 1,4
Millingen Uc=7 m/s	Slope test section 1 and 2	Not reached	Not reached	Overload = 818 m^2/s^2 at the end of 200 l/s/m test
	Transition 1:3 to horizontal (test section 1 and 2)	1 hour into 200 l/s/m test	5 hour into 200 l/s/m test	α = 1,12
	Transition road - grass	-	-	No appropriate α was determined*
* test results will have to give insight in determining a method for determining an α for transitions between grass and road on a dike crest.				

Table 5.5 Summary of prediction of failure during wave overtopping tests at MIllingen aan de Rijn and Nijmegen

5.6 References

Bakker, J. 2012. Graszodetrekproeven Millingen; Nijmegen en Zwolle (Memo).

Emmerling, A., 1973. Die momentane Struktur des Wanddruckes einer turbulenten Grenzschichtströmung, Max-Planck-Institut für Strömungsforschung, Bericht 9.

Hoffmans, G.J.C.M., 2012. The influence of turbulence on soil erosion, Eburon, Delft.

Paulissen, M.P.C.P., 2010. Personal communications.

Schaffers, A.P., Frissel, J.Y., Van Adrichem, M.H.C., Huiskes, H.P.J., Paulissen, M.P.C.P., 2011. Doorworteling dijken ook buiten wintermaanden te meten. Land en Water Nr. 1-2, p. 28-29.

Van Adrichem, M.H.C., 2012. Raw data on root densities on the test locations near Nijmegen and Millingen (Excel file).

Van Ooijen et al., 1996. Technical Report Clay for Dikes, TAW, Rijkswaterstaat, Delft.

6 Conclusions

The last few years, several prototype experiments with the wave-overtopping simulator were carried out to investigate the resistance to erosion of grass revetments. These tests provided insight in both the load and the strength parameters. The overload method is developed and describes the damage at the inner slope of the dike for three different conditions (initial damage, damage at several locations and dike failure). To predict the damage number information is needed about the storm conditions, that is the number of waves and the conditions of the waves (wave height and wave period; here expressed in terms of volume). Moreover, the critical flow velocity of the grass revetment has to be known.

Simple relations are deduced for calculating the flow velocities and flow depths (U and h are correlated to V). The load modelling is extended with the theories of Schuttrumpf and Hughes, which provides insight in the acceleration and deceleration of the flow on the inner slope. At present the best guess value of the friction factor is f = 0.01.

The critical flow velocity depends on the soil properties. The most relevant parameter is the root intensity. Simple relations for Uc and the quality of the grass revetment are available. However, the following research activities are recommended, which are listed below

1) Repeat the grass sod tensile-stress tests during winter conditions (2012-2013) (in order to verify the influence of suction pressures on U_c).
2) Measure the lift force as function of the deformation. Probably the critical lift force as observed by Infram agrees with a deformation that is not realistic for failure.
3) Investigate the root properties, that is determine the mean values and the standard deviations of $\sigma_{root,c}$ and d_r at different depths below the soil surface.
4) Measure the pressure fluctuations both near the bed and at about 5 cm beneath the soil surface (in order to verify the decrease of the load with the depth).
5) Measure the pressure fluctuations at different locations of the slope (in order to verify the decrease of turbulence intensities along the slope). Note that if the velocities increase the turbulence decreases and vice versa.
6) Verify the decrease of the load (pressure fluctuations) in grass covers by using mathematical soil models.
7) Develop a conceptual model that predicts α_M for transitions (from grass revetments to concrete edges and vice versa).
8) Evaluate the exponential decrease of the root intensity. At larger depth, the root intensity is almost linear. Compare both approaches in the strength modelling.

Relevant symbols

a	coefficient (-)
A_i	cross sectional area (m^2)
b	coefficient (-)
C	Chezy coefficient ($m^{0.5}/s$)
D	damage number (m^2/s^2)
f	friction coefficient (-)
F_i	force (N)
h	flow depth (m)
H_s	wave height (m)
p_m	maximum pressure fluctuation (N/m^2)
p_w	suction pressure (N/m^2)
P	probability distribution
q	wave discharge (l/s per unit width)
r_0	relative turbulence intensity (-)
s_{op}	wave steepness (-)
S_b	energy slope or steepness of dike slope (-)
T_p	wave period (s)
U	flow velocity (m/s)
U_c	critical flow velocity (m/s)
V	wave volume (m^3)
z	vertical coordinate (m)
α_M	amplification factor (-)
λ_{ref}	reference height (m)
τ_i	(bed) shear stress (N/m^2)
σ_i	(grass) normal stress (N/m^2)
Ψ	Shields parameter (-)

A Amplification factor

Erosion near trees

The flow pattern around a (bridge) pier can be divided into four characteristic features, namely the bow wave (or surface roller), the down flow, the horseshoe vortex and the wake zone with the shed vortices (or vortex street) (Fig. A1). The flow decelerates as it approaches the pier and comes to rest at the face of the pier. Near the surface, the deceleration is greatest, and decreases downwards. The down flow reaches a maximum just below the bed level. The development of the scour hole around the pier also gives rise to a lee eddy, known as the horseshoe vortex. The horseshoe vortex is effective in transporting particles and extends downstream, past the sides of the pier. The flow separates at the sides of the pier leading to the development of shed vortices in the interface between the flow and the wake.

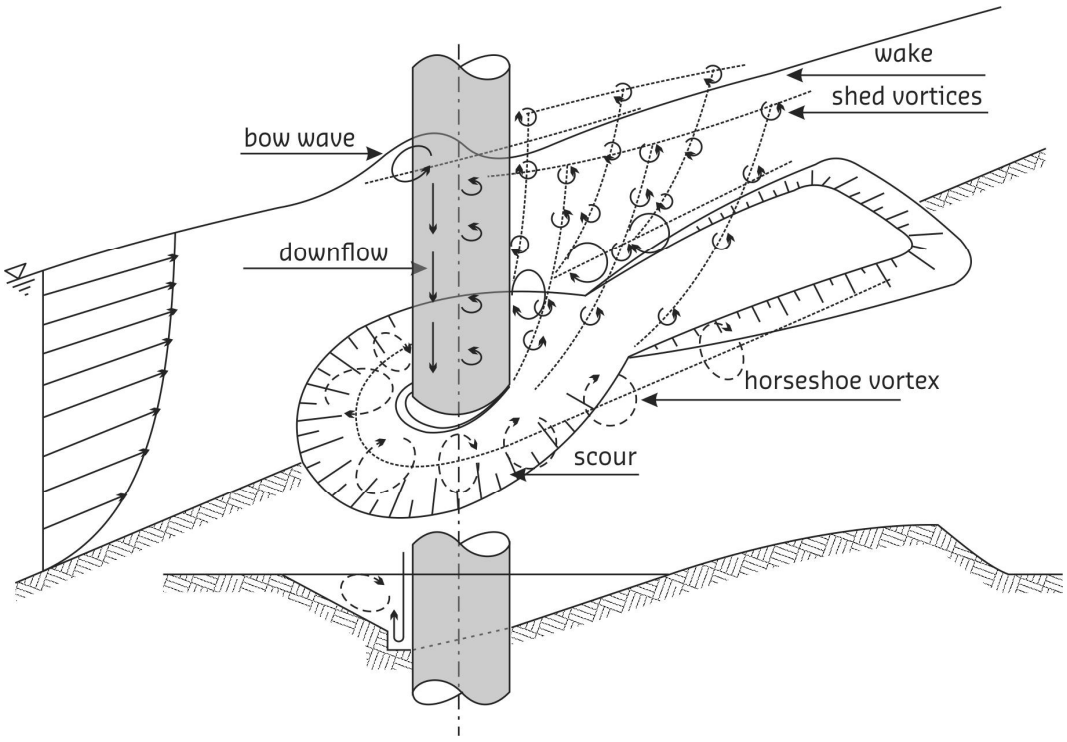

Figure A.1 Characteristic flow zones around bridge pier

The following starting points are made for modelling the erosion process at trees

- Prototype tests at Dutch dikes have shown that the erosion process of grass covers is negligible at slender trees (diameter is less than 15 cm);
- At relative thick trees, whose trunk thickness varies from 0.15 m to 1 m (e.g. tree on the Vechtdijk), limited erosion was observed after a series of storms, so these situations are further considered (Figs A2 and A3);
- Erosion resistance of grass near trees and the erosion resistance of grass on the inner dike slope are assumed equal. In practice, due to shadow effects the grass strength near trees is less;
- For laminar flow conditions, the flow velocity alongside the object is two times as large as the upstream flow velocity (potential theories): $\alpha_M = 2$. When the flow is turbulent and supercritical $\alpha_M < 2$ (Fig. A4);

- Practical tests have shown that downstream of thick trees there will be no directly mixing of water (Fig. A5). Consequently, the load of the accelerated water along the tree is decisive with respect to the load of the downstream turbulence.

Figure A.2 Erosion at tree; width of test section is 4 m

Figure A.3 Erosion at tree; width of test section is 4 m

- To model the influence of trees on the erosion process an amplication factor is defined as the ratio between the flow velocity at the tree and the flow velocity upstream of the tree. Note that the application of the force balance is effective only if equilibrium situations are considered. Because the erosion process close to the tree is not yet in equilibrium no analytical solution can be deduced due to acceleration terms in the balance of forces.

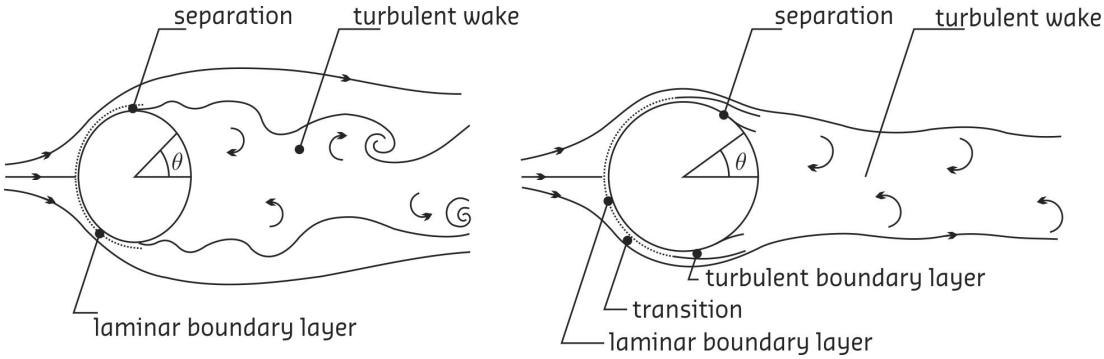

Figure A.4 LEFT Sub-critical flow at pile, RIGHT Supercritical flow at pile

Figure A.5 Downstream of tree (there is no mixing downstream of the tree)

Defining a control volume with an inflow section upstream of the tree (denoted with subscript 1) and an outflow section at the tree (denoted with subscript 2), the application of the continuity equation gives (Fig. A6)

$$Q_1 = Q_2 \qquad \text{(A1)}$$

where

$$Q_1 = U\ell h\left(1-\eta_a\right) \qquad \text{(A2)}$$

and

$$Q_2 = U_{tree}\left(\ell - b\right)h\left(1-\eta_{a,1}\right)+U_{tree,2}\left(\ell - b\right)\left(h_2 - h\right)\left(1-\eta_{a,2}\right) \qquad \text{(A3)}$$

in which b is the width of the tree/pier, h is the flow depth at the inflow section, h_2 is the flow depth at the outflow section. The length scale ℓ (≈ 3 to 5 times h) represents the width of the scour hole (e.g. Hoffmans and Verheij 1997). At the inflow section U is the depth-averaged flow velocity, U_{tree} represents the depth-averaged flow velocity at the outflow section in the lower part of the flow, $U_{tree,2}$ is the depth-averaged flow velocity at the outflow section in the upper part of the flow and η_a is the air content. The discharge at the inflow section is given by Q_1 and Q_2 is the discharge at the outflow section

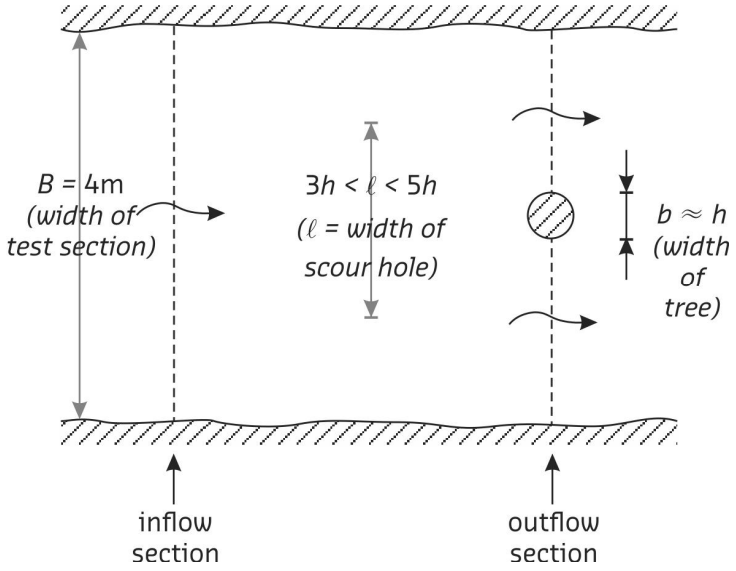

Figure A.6a Top view of test section

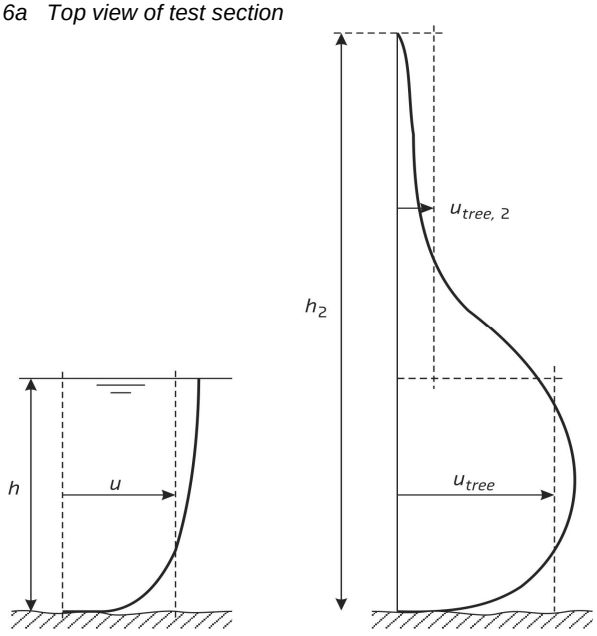

Figure A.6b Vertical flow velocity distributions at inflow and outflow sections

Because of the flow impact at the tree, the flow velocities just before the tree decrease significantly. Hence, at the outflow section the flow velocities above the upstream water surface are relatively low with respect to the depth-averaged flow velocity upstream of the tree ($U_{tree,2}$ << U). Most likely, the aeration in the upper part of the flow is relatively high in comparison to the aeration upstream (η_a << $\eta_{a,2}$). Therefore, Eq. A3 can be approximated by

$$Q_2 = U_{tree}\left(\ell - b\right)h\left(1-\eta_{a,1}\right) \tag{A4}$$

Assuming that $\eta_a = \eta_{a,1}$ it follows from Eqs. A1, A2, A3 and A4

$$U\ell = U_{tree}\left(\ell - b\right) \tag{A5}$$

By using

$$U_{tree} = \alpha_M U \tag{A6}$$

the increase of the flow velocity or the amplification factor (α_M) can be estimated by

$$\alpha_M = \frac{\ell}{\ell - b} \tag{A7}$$

A first approximation yields for $\ell = 4h$ (and $b \approx h$ m)

$$\alpha_M = \frac{\ell}{\ell - b} = \frac{4h}{4h - h} = 1.3 \tag{A8}$$

This value of α_M agrees approximately with the experimental value for round piers as proposed by Melville (1975) (Fig. A7)

$$\alpha_M = U_{pier}/U = 1.2 \tag{A9}$$

where U_{pier} is the depth-averaged flow velocity along the tree/pier (Note that $U_{pier} = U_{tree}$).

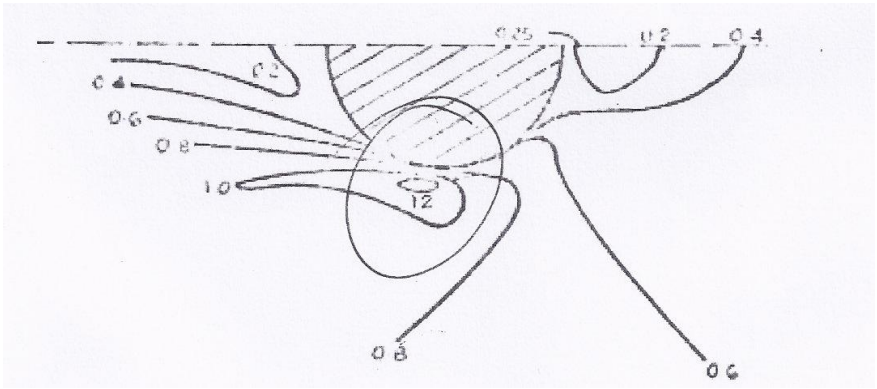

Figure A.7 Flow velocities at a bridge pier relative to the approach velocity (Melville 1975)

Since the amplification factor also depends on the shape of the pier a more general relation can be given (e.g Hoffmans and Verheij 1997)

$$\alpha_M = 1.2 K_{shape} \qquad \text{(A10)}$$

where K_{shape} is the shape factor of an obstacle (-) which varies from 0.8 (elliptic form) to 1.2 (rectangular form). Consequently, the amplification factor ranges from 1 to 1.5.

When α_M = 1.0 (no obstacle) it follows from Table A1 that $D \approx 1000$ m^2/s^2 or at several locations erosion occurs which is acceptable since the residual strength is not yet applied. However, if α_M = 1.5 due to obstacles then $D \approx 3000$ m^2/s^2 (Table A1) and so significantly more erosion is expected. Assuming that α_M = 2 dike failure may occur ($D \approx 5500$ m^2/s^2).

It is concluded on the above approach that the amplification factor α_M for relatively large obstacles is in the range of 1.0 to 1.5.

Erosion at a transition of a slope to a horizontal berm

The situation at a transition can be compared with a jet that normally occurs because of flow under, through or over hydraulic structures. In general, a jet lifts soil and transports it downstream of the impacted area. The jet impact area is transformed into an energy dissipater and a scour hole is formed (Fig. A8). Based on physical backgrounds, the equilibrium scour depth ($z_{m,e}$) for 2D flow conditions and for loose packed materials is (Hoffmans and Verheij 1997 and Hoffmans 2012)

$$2DV \qquad z_{m,e} = z_{2DV} = c_{2DV}\sqrt{\frac{qU}{g}} \qquad \text{(A11)}$$

and

$$2DH \qquad z_{m,e} = z_{2DH} = c_{2DH}\sqrt{\frac{qU}{g}} \qquad \text{(A12)}$$

where

$$c_{2DV} = \frac{20}{\left(D_{90*}\right)^{1/3}} \quad \text{for} \quad 25 < D_{90*} < 250 \quad \text{or} \quad 1 \text{ mm} < d_{90} < 10 \text{ mm} \qquad \text{(A13)}$$

and

$$c_{2DH} = \frac{20}{\left(D_{90*}\right)^{1/2}} \quad \text{for} \quad 25 < D_{90*} < 250 \quad \text{or} \quad 1 \text{ mm} < d_{90} < 10 \text{ mm} \qquad \text{(A14)}$$

with

$$D_{90*} = d_{90}\left(\frac{\Delta g}{\nu}\right)^{1/3} \qquad \text{(A15)}$$

where c_i is a dimensionless parameter depending on the particle diameter (Fig. A9), d_{90} is the particle diameter for which 90% of the sediment particles is finer than d_{90}, g is the acceleration of gravity, q is the discharge per unit width, U is the jet velocity, $z_{m,e}$ is the equilibrium scour depth, Δ is the relative density and ν is the kinematic viscosity.

V (ℓ/m)	U (m/s)	α_M = 1	α_M = 1.2	α_M = 1.4	α_M = 1.5	α_M = 1.6	α_M = 1.8	α_M = 2.0
200	2.89			0.40	2.83	5.42	11.11	17.47
200	2.89			0.40	2.83	5.42	11.11	17.47
200	2.89			0.40	2.83	5.42	11.11	17.47
400	3.66		3.31	10.28	14.17	18.32	27.44	37.63
400	3.66		3.31	10.28	14.17	18.32	27.44	37.63
400	3.66		3.31	10.28	14.17	18.32	27.44	37.63
600	4.20	1.66	9.44	18.62	23.74	29.22	41.23	54.65
600	4.20	1.66	9.44	18.62	23.74	29.22	41.23	54.65
600	4.20	1.66	9.44	18.62	23.74	29.22	41.23	54.65
800	4.63	5.48	14.93	26.10	32.33	38.99	53.60	69.92
800	4.63	5.48	14.93	26.10	32.33	38.99	53.60	69.92
800	4.63	5.48	14.93	26.10	32.33	38.99	53.60	69.92
800	4.63	5.48	14.93	26.10	32.33	38.99	53.60	69.92
1000	5.00	9.00	20.00	33.00	40.25	48.00	65.00	84.00
1000	5.00	9.00	20.00	33,00	40.25	48.00	65.00	84.00
1000	5.00	9.00	20.00	33.00	40.25	48.00	65.00	84.00
200	2.89			0.40	2.83	5.42	11.11	17.47
1000	5.00	9.00	20.00	33.00	40.25	48.00	65.00	84.00
1000	5.00	9.00	20.00	33.00	40.25	48.00	65.00	84.00
1000	5.00	9.00	20.00	33.00	40.25	48.00	65.00	84.00
2000	6.33	24.05	41.68	62.50	74.12	86.54	113.77	144.21
2000	6.33	24.05	41.68	62.50	74.12	86.54	113.77	144.21
2000	6.33	24.05	41.68	62.50	74.12	86.54	113.77	144.21
3000	7.26	36.77	59.99	87.43	102.73	119.09	154.97	195.08
3000	7.26	36.77	59.99	87.43	102.73	119.09	154.97	195.08
3000	7.26	36.77	59.99	87.43	102.73	119.09	154.97	195.08
4000	8.01	48.17	76.41	109.78	128.39	148.28	191.91	240.69
4000	8.01	48.17	76.41	109.78	128.39	148.28	191.91	240.69
4000	8.01	48.17	76.41	109.78	128.39	148.28	191.91	240.69
5000	8.64	58.69	91.55	130.38	152.04	175.20	225.98	282.74
5000	8.64	58.69	91.55	130.38	152.04	175.20	225.98	282.74
5000	8.64	58.69	91.55	130.38	152.04	175.20	225.98	282.74
5500	8.93	63.69	98.75	140.19	163.30	188.00	242.19	302.75
5500	8.93	63.69	98.75	140.19	163.30	188.00	242.19	302.75
5500	8.93	63.69	98.75	140.19	163.30	188.00	242.19	302.75
1000	5.00	9.00	20.00	33.00	40.25	48.00	65.00	84.00
2000	6.33	24.05	41.68	62.50	74.12	86.54	113.77	144.21
3000	7.26	36.77	59.99	87.43	102.73	119.09	154.97	195.08
4000	8.01	48.17	76.41	109.78	128.39	148.28	191.91	240.69
5000	8.64	58.69	91.55	130.38	152,04	175.20	225.98	282.74
Damage number (m^2/s^2)		**944**	**1609**	**2405**	**2855**	**3337**	**4393**	**5574**

Table A1 Experimental values Vechtdijk V (wave volume (ℓ/m), U and U_c = 4 m/s and computational results of the overload method (α_M and D)

Figure A8 Scour hole at the toe of the dike; sub soil consists of gravel (Kattendijke)

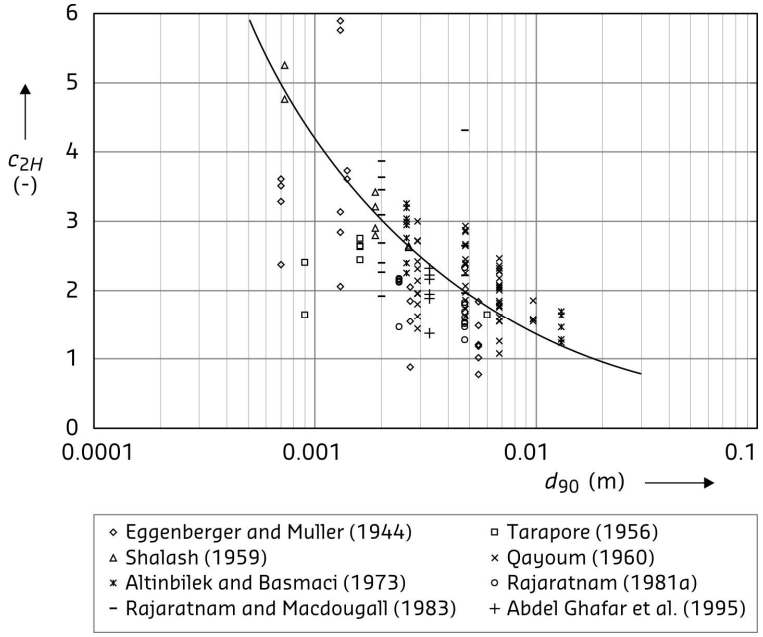

Figure A9 The inverse strength versus particle diameter for 2D-H flow conditions (Hoffmans 2012)

If the discharge and/or the jet velocity increase then the load also increases which results in greater scour depths. Considering a vertical and a horizontal jet with equal load conditions (thus $q_{2DV} = q_{2DH}$ and $U_{2DV} = U_{2DH}$) the scour dimensions for 2D-V jets are approximately two times bigger. Note that the ratio between c_{2DV} and $2c_{2DH}$ is

$$\frac{c_{2DV}}{c_{2DH}} = \frac{20}{\left(D_{90*}\right)^{1/3}} \cdot \frac{\left(D_{90*}\right)^{1/2}}{20} = \left(D_{90*}\right)^{1/6} \approx 2 \quad \text{for} \quad 25 < D_{90*} < 250 \qquad \text{(A16)}$$

For oblique jets holds

$$z_{m,e} = z_{2DO} = c_{2DV}\sqrt{\frac{qU\sin\beta}{g}} \quad \text{for} \quad 15^0 < \beta < 90^0 \tag{A17}$$

and

$$z_{m,e} = z_{2DO} = c_{2DH}\sqrt{\frac{qU}{g}} \qquad \text{for} \quad 0^0 < \beta \le 15^0 \tag{A18}$$

where β is the angle between the jet and the horizontal (or the angle of the inner dike slope), For $\beta = 15^o$ (or slope steepness is 1V:4H) holds

$$c_{2DV}\sqrt{\frac{qU\sin 15^0}{g}} = c_{2DH}\sqrt{\frac{qU}{g}}$$

or

$$\frac{c_{2DV}}{c_{2DH}}\sqrt{\sin 15^0} = 1$$

or

$$2\sqrt{0.25} = 2\cdot \tfrac{1}{2} = 1 \tag{A19}$$

Consequently, for slopes gentler than 1V:4H no extra erosion is expected at the transition of the dike slope to the horizontal berm. Since the discharge can be written as

$$q = Uh \tag{A20}$$

where *h* is the width of the jet (or the flow depth) the equilibrium scour depth is proportional to

$$z_{m,e} \equiv U \tag{A21}$$

To estimate the increase of scouring of oblique jets with respect to horizontal jets the amplification ratio is a function of z_{2DO} and z_{2DH}. As α_M is related to *U* (see also Eqs. A6 and A9) the amplification factor for erosion at the transition can be approximated by

$$\alpha_M = \frac{z_{2DO}}{z_{2DH}}$$

or

$$\alpha_M = 2\sqrt{\sin\beta} \quad \text{for} \quad 15^0 < \beta < 90^0 \tag{A22a}$$

and

$$\alpha_M = 1 \quad \text{for} \quad 0 < \beta \le 15^0 \tag{A22b}$$

When the slope steepness is 1V:2.7H (or $\beta = 20^o$) yields

$$\alpha_M = 2\sqrt{\sin 20^o} = 1.2 \tag{A23}$$

If β = 35^o (or slope steepness is 1V:1.4H) then α_M = 1.5. Hence, the best guess value of the amplification factor for this flow type varies from 1.0 to 1.5 so more erosion could occur near the toe (see also Fig. A8). Values for *D* for various values of α_m are shown in Table A1.

Summarizing, two conceptual models are discussed for predicting the erosion at obstacles (or trees) and at transitions of dike slope to berms. The amplification factor represents the relative increase of the flow velocity. To determine the erosion the overload method is extended by

$$\sum_{i=1}^{N}\left(\alpha_M U_i\right)^2 - U_c^2 = D \qquad \text{(A24)}$$

where *U* represents the flow velocity of the overtopping wave, U_c is the critical depth-averaged flow velocity and *N* is the number of the waves in which $U > U_c$. Finally, it is noted that the amplification factor must also be determined for houses, stairs and other types of obstacles, which are not discussed in this Appendix.

References

Hoffmans, G.J.C.M., 2012. The Influence of Turbulence on Soil Erosion, Deltares Select Series Volume 10, Eburon, Delft.

Hoffmans, G.J.C.M. and Verheij, H.J., 1997. Scour Manual. Balkema, Rotterdam.

Melville, B., 1975.

B Root investigation

The table below gives a description of the sod appearance (see also Chapter 4):

plot	% total	% grasses	% herbs	mean crop height (cm)	manure visible	litter	molehills per 25 m^2
Hollands-Duits gemaal 1	70	65	25	5	No	Mown litter	2
Hollands-Duits gemaal 2	65	60	20	10	No	-	2
Hollands-Duits gemaal 3	70	60	15	15	No	Mown litter	1
Millingen outer slope	99	95	35	20	No	-	2
Millingen inner slope	80	80	25	40	No	-	0

In the following Figs B1 to B5, the average root density in the five sample plots is shown according to the gouge auger method prescribed by the third assessment round (V&W, 2007) and extended for the purpose of our measurements to a depth of 50 cm. In Tables 4.1 and 4.2 (Chapter 4), the final quality verdict according to this method is shown. According to V&W (2007), the coloured zones in Figs B1 to B5 represent different root density qualities: purple = very poor; red = poor; orange = moderate; green = good.

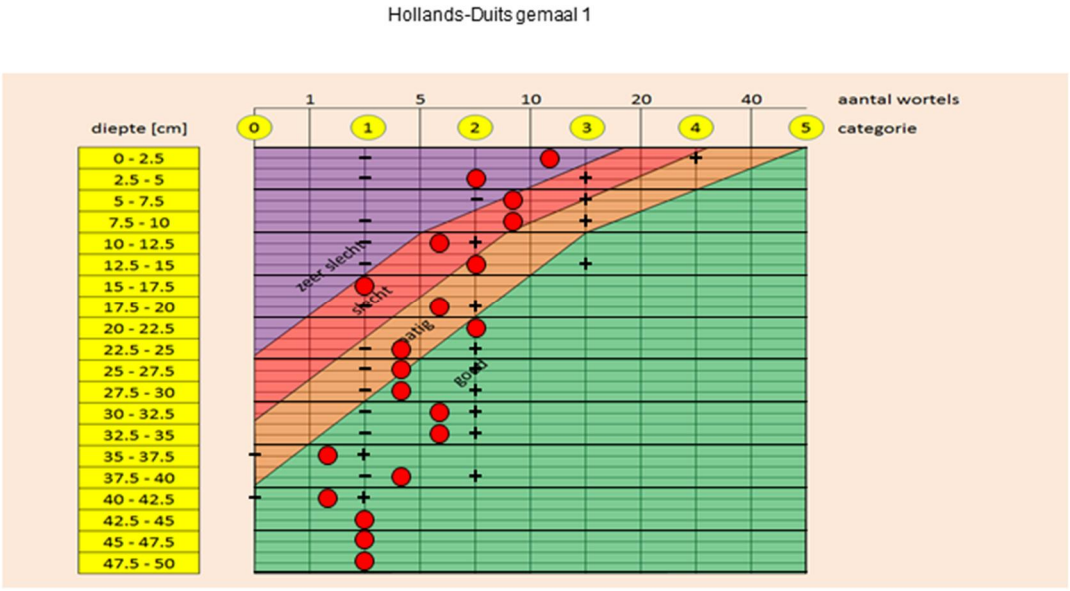

Figure B.1 Root densities according to gouge auger method (n = 3) in sample plot 1 on the inner slope near the Hollands-Duits gemaal. For every depth layer, the range of measured values is indicated by + (highest value found) and – (lowest value found)

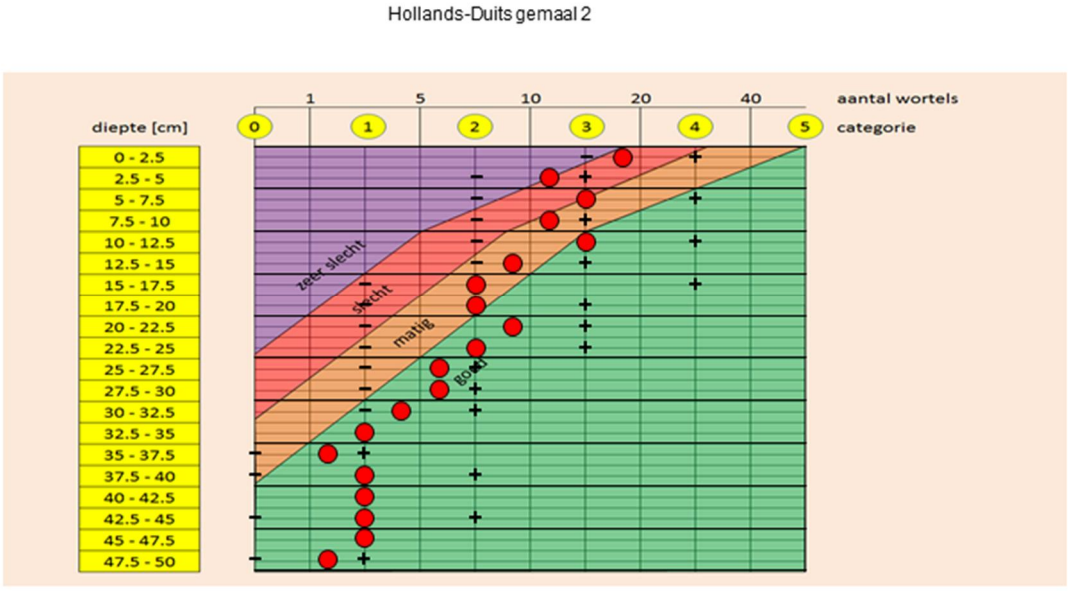

Figure B.2 *Root densities according to gouge auger method (n = 3) in sample plot 2 on the inner slope near the Hollands-Duits gemaal. For every depth layer, the range of measured values is indicated by + (highest value found) and – (lowest value found)*

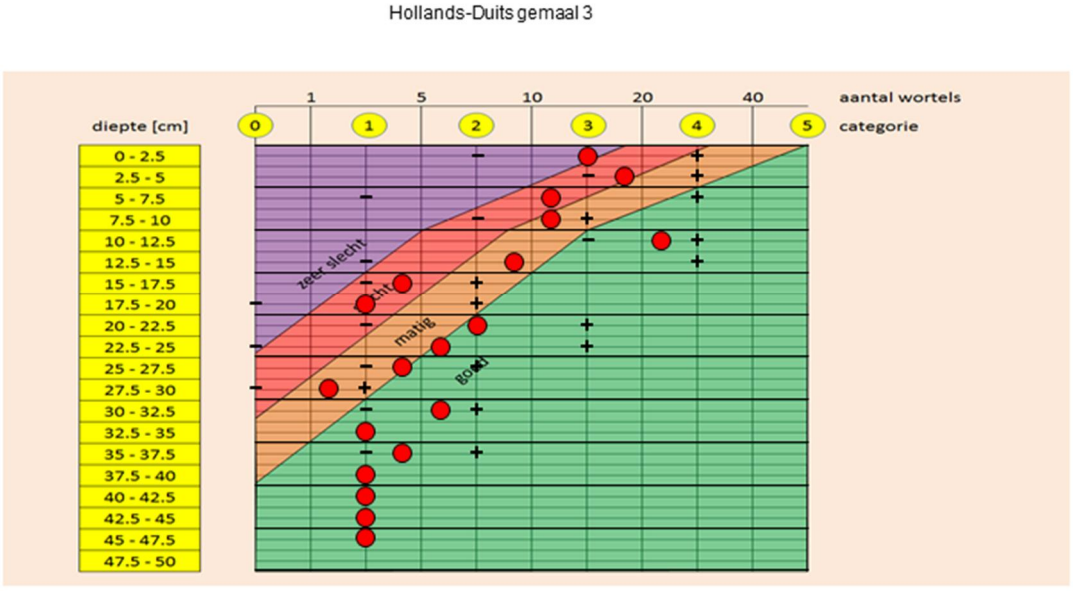

Figure B.3 *Root densities according to gouge auger method (n = 3) in sample plot 3 on the inner slope near the Hollands-Duits gemaal. For every depth layer, the range of measured values is indicated by + (highest value found) and – (lowest value found)*

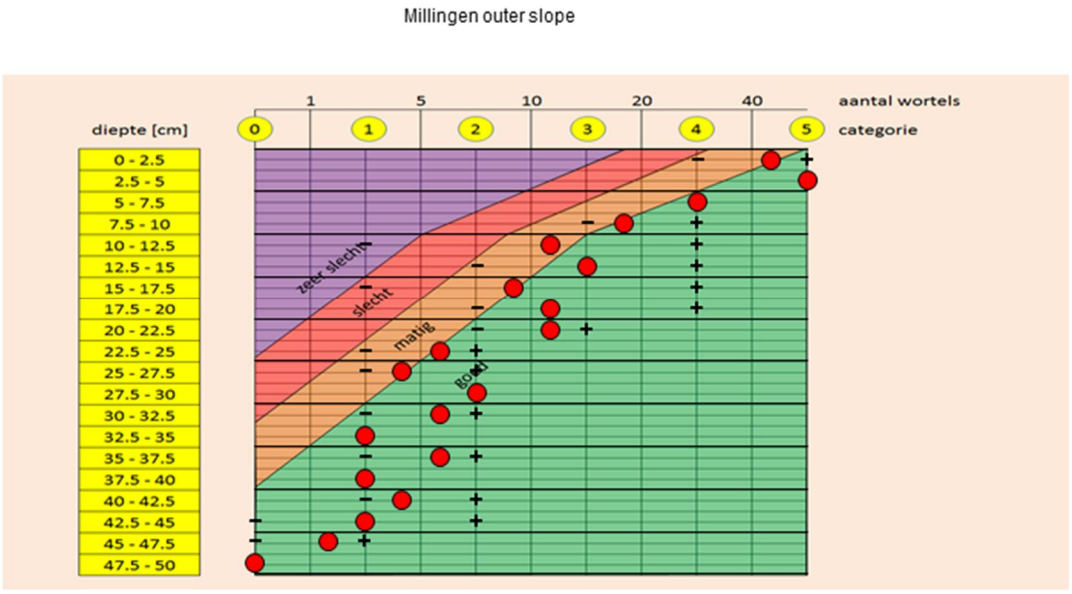

Figure B.4 *Root densities according to gouge auger method (*n = *3) on the outer slope near Millingen. For every depth layer, the range of measured values is indicated by + (highest value found) and – (lowest value found)*

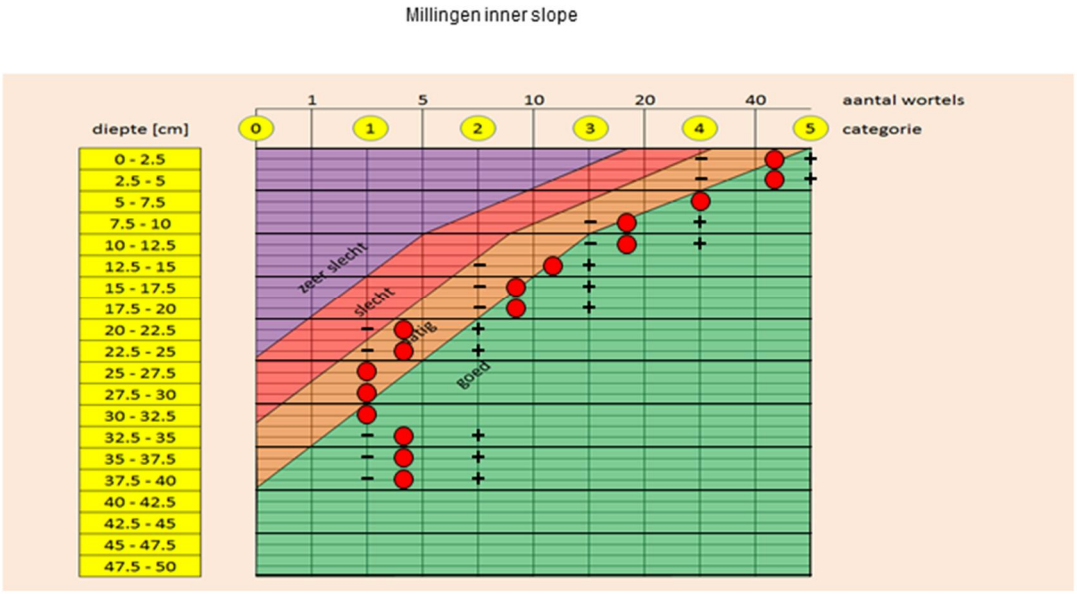

Figure B.5 *Root densities according to gouge auger method (*n = *3) on the inner slope near Millingen. For every depth layer, the range of measured values is indicated by + (highest value found) and – (lowest value found)* B-3B-3

C Root model

Soil structure has a major influence on water and air movement, biological activity and root growth. A structured soil has many variously shaped spaces including tunnels. In the uppermost decimetres under the turf on a dike bank the soil structure is usually very strongly developed and consists of relatively small aggregates with dimensions of millimetres to centimetres. The aggregates are often linked to each other by roots. At greater depths under the grass cover the aggregates are often less clearly recognizable. There the dimensions are sometimes more than 1 dm and there is often still some cohesion present between the aggregates.

The Mohr-Coulomb equation describes the shear failure of soil in terms of shear stresses as well as normal stresses and can be written as (e.g. Lambe and Whitman 1969)

$$\tau_s = c_e \cos\phi_e + (\sigma - p_w)\sin\phi_e \qquad \text{(C1)}$$

where c_e is the effective (soil) cohesion, p_w is the pore water pressure, σ is the soil normal stress, τ_s is the soil shear stress and ϕ_e represents the effective internal friction angle. The magnitude of σ depends on the weight of the soil and the water content. For saturated soils, the buoyancy generated by p_w reduces the normal stress. However, for unsaturated soils suction pressures increase the normal stress. For dry soil when p_w = 0 both c_e = c (with c is the cohesion) and ϕ_e equals the internal friction angle (ϕ).

Typically, the strength of roots is modelled by the root cohesion (c_r). In a root-permeated soil Eq. C1 can be modified to include c_r

$$\tau_s = c_e \cos\phi_e + c_r + (\sigma - p_w)\sin\phi_e \qquad \text{(C2)}$$

Most attempts to determine the effects of root reinforcement by grassland vegetation have used root-cohesion estimates according to the root equation of Wu et al. (1979), which requires the mean root tensile stress (σ_{root}) and the mean root diameter (d_{root}). Where a root crosses a shear zone, σ_{root} can be resolved into components parallel ($\sigma_{root,h}$) and perpendicular ($\sigma_{root,v}$) to the shear zone (Fig. C1), thus, c_r is

$$c_r = \frac{A_{root}}{A_1}\left(\sigma_{root,v}\tan\phi + \sigma_{root,h}\right) = \sigma_{root}\frac{A_{root}}{A_1}\left(\cos\theta\tan\phi + \sin\theta\right) \qquad \text{(C3)}$$

where A_{root}/A_1 is the root area ratio also known as RAR (A_{root} is the cross sectional area of No (= number) roots per m^2 and A_1 = 1 m^2) and θ is the angle of shear rotation. Although little is known about θ, from field observations of conifers, Wu et al. (1979) suggested a range of 45^o to 70^o. Since ϕ varies from 30^o to 40^o Eq. C3 is insensitive to changes in θ, c_r may be rewritten as $c_r = 1.2\sigma_{root}A_{root}/A_1$.

Though horizontal roots may have some impacts on the threshold condition for vertical motion, here the mean grass normal stress (σ_{grass}) is approximated by

$$\sigma_{grass} = \frac{A_{root}}{A_1}\left(\sigma_{root,v} + \sigma_{root,h}\tan\phi\right) = \sigma_{root}\frac{A_{root}}{A_1}\left(\cos\theta + \sin\theta\tan\phi\right) \qquad \text{(C4)}$$

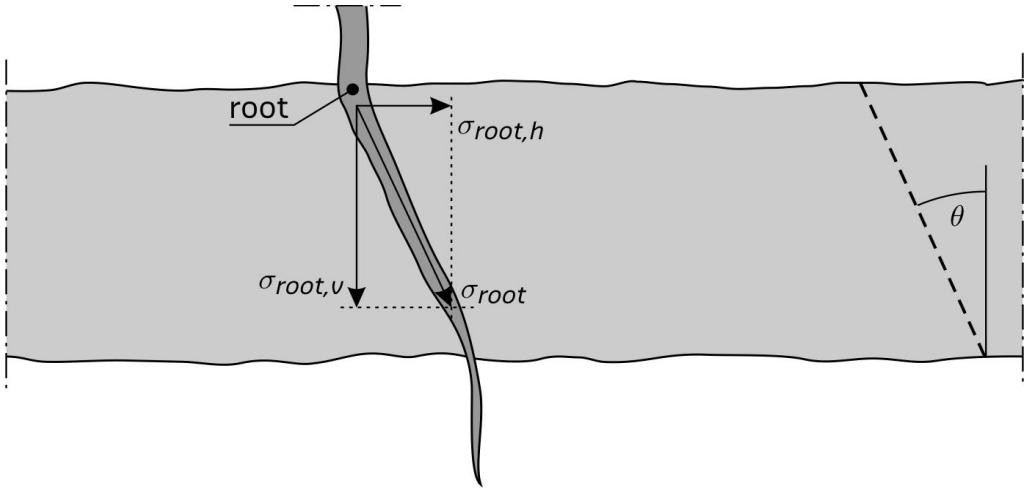

Figure C.1 Well-anchored root

The stresses c_r and σ_{grass} are correlated and do not include the friction of roots on clay. If all roots are well-anchored and if they all have the same properties they will then all break simultaneously during the critical stage. Prototype experiments have demonstrated that the breaking of roots is a dynamic process (Pollen and Simon 2003; Van Hoven et al. 2010) so some roots break, some roots are pulled out owing to a lack of anchoring and some roots are not pulled out. This process is also partly confirmed by Paulissen (2010) who showed that the standard deviation of the critical instantaneous root tensile stress equals about the critical mean root tensile stress.

The critical mean root tensile stress depends strongly on the type and the quality of the grass. Sprangers (1999) measured grass parameters such as the root length and the dry root mass densities from 24 Dutch dike sites. He found that A_{root}/A_1 of dike grassland decreases exponentially with depth and that approximately ⅔ of the roots can be found in the top 10 cm of the turf, while about ¾ of the roots were located within the top 20 cm. The critical mean grass normal stress, which is at maximum near the surface and decreases with depth, is here estimated by

$$\sigma_{grass,c}(z) = \sigma_{grass,c}(0)\exp\left(\frac{z}{\lambda_{ref}}\right) \tag{C5}$$

with $\phi = 30^o$ and $\theta = 60^o$ (see also Eq. C4)

$$\sigma_{grass,c}(0) = \frac{A_{root}(0)}{A_1}\sigma_{root,c} \tag{C6}$$

in which λ_{ref} is a reference height which ranges from 5 cm to 10 cm, $\sigma_{grass,c}(0)$ is the critical mean grass normal stress near the surface and $A_{root}(0)/A_1$ represents the root area ratio close to the surface. For Dutch grasses, the number of roots near the surface lies in the range of 20 to 50 per standard area according to VTV-2006 (or 15000 per m^2 to 60000 per m^2) (Fig. C2).

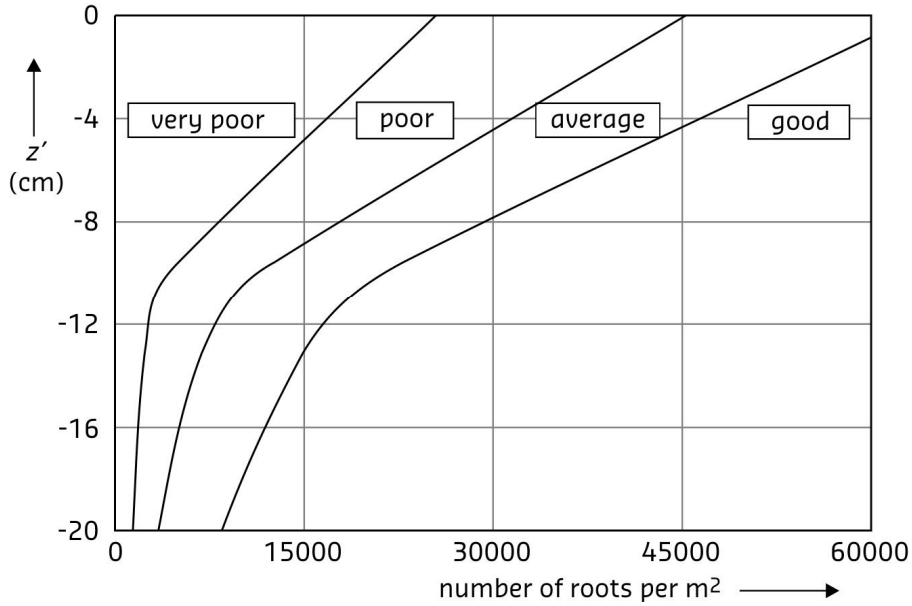

Figure C.2 Classification of grass according to the Dutch guidelines for primary defences

Based on Spranger's work, the Dutch guidelines for assessing primary dikes (VTV 2006) distinguish four different qualities for the grass cover in which the quality of the grass is strongly correlated with the number (No) of roots. In clayey soils the mean root diameter of Dutch grasses is about d_{root} = 0.1 mm (Paulissen 2010), which is significantly finer than the range of d_{root} tested by the Chinese researchers Cheng et al. (2003) (Table C1).

Paulissen (2010) carried out more than 500 laboratory experiments in which the strength of Dutch grasses was tested yielding $\sigma_{root,c} = 15 \cdot 10^6$ N/m^2. If the following assumptions are made: d_{root} = 0.1 mm and $\sigma_{root,c} = 15 \cdot 10^6$ N/m^2 then the root properties can be determined (Table C.2).

Type of grass	d_{root} (mm)	RMS of d_{root}	$\sigma_{root,c}$ (x 10^6 N/m^2)	RMS of $\sigma_{root,c}$
Late Juncellus sp.	0.38	0.43	24.50	4.20
Dallis grass	0.92	0.28	19.74	3.00
White Clover	0.91	0.11	24.64	3.36
Vetiver	0.66	0.32	85.10	31.2
Common Cetipede grass	0.66	0.05	27.30	1.74
Bahia grass	0.73	0.07	19.23	3.59
Manila grass	0.77	0.67	17.55	2.85
Bermuda grass	0.99	0.17	13.45	2.18

Table C.1 Indicative strength parameters of different grasses (Cheng et al. 2003)

Grass quality VTV-2006	(1) No(0) per VTV area	(2) $A_{root}(0)/A_1$ (-)	(3) $A_1/\mathrm{No}(0)$ (mm^2)	(4) $A_1/\mathrm{No}(0)^{½}$ (mm)	(5) $\sigma_{grass,c}(0)$ (kN/m^2)
very poor	< 18	< 0.0002	> 39	> 6	< 3.0
poor	18 – 32	0.0002 – 0.0004	22 – 39	5 – 6	3.0 – 5.3
average	32 – 45	0.0004 – 0.0005	16 – 22	4 – 5	5.3 – 7.5
good	> 45	> 0.0005	< 16	< 4	> 7.5

(1) No(0) is the number of roots per VTV area near the surface; No (= $A_{root,VTV}/A_{1\ root}$); $A_{root,VTV}$ is the cross-sectional area of all roots per $¼\pi d_b^2$ with d_b = 0.03 m and A_{1root} [$=¼\pi(d_{root})^2$] is the cross-sectional area of a single root with d_{root} = 0.1 mm;

(2) $A_{root}(0)/A_1$ is the root area ratio near the surface with A_1 = 1 m^2;

(3) $A_1/\mathrm{No}(0)$ is the turf area per root near the surface;

(4) $A_1\mathrm{No}(0)^{½}$ is the root spacing near the surface;

(5) see also Eq. C6 by using $\sigma_{root,c} = 15\cdot10^6$ N/m^2.

Table C.2 Root properties of Dutch dike grassland (near the surface)

References

Cheng, H., Yang, X., Liu, A., Fu, H., Wan, M., 2003. A study on the performance and mechanism of soil-reinforcement by herb root system. *Proc. of the* 3rd *Int. Conf. on Vetiver and Exhibition,* Guangzhou, China.

Lambe, T.W., Whitman, R.V., 1969. *Soil Mechanics*. John Wiley, New York.

Paulissen, M.P.C.P., 2010. Personal Communications. Alterra, Wageningen University and Research Centre, The Netherlands.

Pollen, N.L., Simon, A., 2003. A new Approach for Quantifying Root-Reinforcement of Streambanks: the RipRoot, American Geophysical Union, Fall Meeting 2003, abstract #H52A-1174.

Sprangers, J.T.C.M., 1999. Vegetation dynamics and erosion resistance of sea dyke grassland, *Doctoral Thesis*, Wageningen Agriculture University, Wageningen, The Netherlands.

Van Hoven, A., Van der Meer, J.W., Verheij, H.J., Hoffmans, G.J.C.M., Paulissen, M.P.C.P., Steendam, G.J., Akkerman, G.J., 2010. Investigation of erodibility and stability of grass covers [in Dutch], (Deltares projects: 1001187; 1001188, 1001189, 1200259, 1201541, 1202126, 1204204), Deltares, Delft.

VTV, 2006. *Safety assessment of the primary flood defences* [in Dutch], Ministry of Transport, Public Works and Water Management, Rijkswaterstaat, Delft.

Wu, T.H., McKinnell, W.P. III, Swanston, D.N., 1979. Strength of tree roots and landslides on Prince of Wales Island, Alaska. *Canadian J. of Geotechnical Res.* 16(l), 19-33.

D Turf-element model

If in the saturated zone, a turf aggregate with the dimensions of a cube is considered, the following forces acting on this cube can be distinguished: the load due to the lift force caused by pressure fluctuations perpendicular to the grass cover, and the strength, i.e., the submerged weight of the soil, and the frictional and tensile forces. Figure D1 shows a cube $\ell_x\ell_y\ell_z = \ell^3$ at a horizontal plane where ℓ_x, ℓ_y and ℓ_z are length scales in the x, y and z direction respectively and ℓ is the representative aggregate scale. The turf aggregate is unstable if the load is greater than the strength, thus

$$F_p \geq F_w + 4F_c + F_t \tag{D1}$$

where

$$4F_c = 2(1-n)\left(C_{clay,c} + \tau_{grass,c}\right)\left(\ell_x + \ell_y\right)\ell_z \tag{D2}$$

$$F_p = p_m \ell_x \ell_y \tag{D3}$$

$$F_t = (1-n)\left[C_{clay,c} + \sigma_{grass,c}\left(z = -\ell_z\right)\right]\ell_x\ell_y \tag{D4}$$

$$F_w = (1-n)\left(\rho_s - \rho\right) g \ell_x \ell_y \ell_z \tag{D5}$$

where F_c is the critical frictional force, whichs act on one sidewall and depends on the critical rupture strength of clay ($C_{clay,c}$) and the critical mean grass shear stress ($\tau_{grass,c}$) of the intersected roots per side wall averaged over ℓ_z, F_p is the maximum lift force, F_t is the critical mean tensile force on the bottom-element, F_w is the submerged weight of the soil, n (≈ 0.4) is the porosity, ρ is the fluid density and ρ_s is the density of soil (for quartz $\rho_s \approx 2650$ kg/m^3).

The assumption of Eq. D1 is applicable if p_m at the top of the turf aggregate significantly decreases with depth or if the penetration length (L_d) is $L_d/\ell \ll 1$. According to De Groot et al. (1996) and Bezuijen and Köhler (1996)

$$L_d = \sqrt{\frac{c_v T_p}{\pi}} \tag{D6}$$

where c_v is the consolidation coefficient and T_p is the pressure period of the vortices in the turbulent flow at the inner slope of the dike.

For uniform and turbulent flow conditions T_p varies from $T_p = 0.1$ s (eddies at micro scale) to $T_p = 1$ s (eddies at macro scale). If the order of magnitude of c_v is $O(c_v) = 10^{-3}$ m^2/s and $O(T_p) = 1$ s, then $O(L_d) = 0.01$ m, thus the pore pressure variation equals the total stress variation at a depth greater than one or two times L_d. Based on measured flow fluctuations in open pores of granular filters under uniform and sub-critical flow conditions Klar (2005) found that the turbulence energy at 5 cm below the bed level is about 10% of the bed turbulence energy. Hence, also from a hydraulic engineering approach the penetration length is limited. By using $\ell_x = \ell_y = \ell_z = -z$, Eq. D1 can be rewritten as

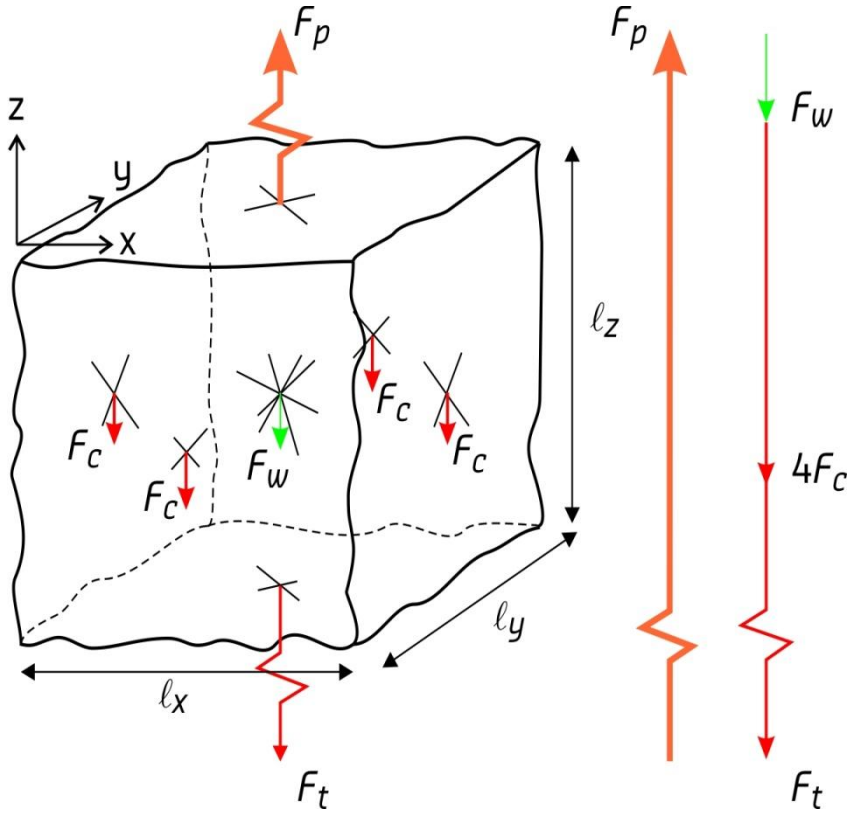

Figure D.1 Forces acting upon a turf element

$$p_m \geq \sigma_{soil}(z) = -(1-n)\left[(\rho_s - \rho)gz - 4\left(C_{clay,c} + \tau_{grass,c}\right) - \left(C_{clay,c} + \sigma_{grass,c}(z)\right)\right] \quad \text{(D7)}$$

where $\sigma_{soil}(z)$ is the soil normal stress as function of z. If the location of the minimum soil normal stress lies within the turf and if the load is sufficiently high bulging mechanisms occur, otherwise the grass cover gradually erodes. Figure D2 shows a bulging turf aggregate at the Boonweg in Friesland (Van der Meer 2008) where $p_m > \sigma_{soil}(\lambda_{ref})$.

When describing incipient motion, horizontal forces are usually considered. The critical condition for moving turf aggregates is reached when τ_0 equals the critical mean bed shear stress (τ_c). If there is neither clay nor grass, neglecting the frictional forces acting on the side walls, τ_c of loosely packed materials is ($z = -d$)

$$\tau_c = \Psi_c(\rho_s - \rho)gd \quad \text{(D8)}$$

with

$$\Psi_c = \alpha_\tau^{-1}(1-n) = \tfrac{1}{18}(1-0.4) = 0.033 \quad \text{(D9)}$$

where d is the particle diameter. In turbulent flow, the critical Shields parameter (Ψ_c) varies from 0.03 (occasional particle movement at some locations) to 0.06 (general transport) for coarse sand and gravel, whereas for small Reynolds numbers up to fully laminar flow Ψ_c can reach values up to 0.15. Hence, the first term on the right side in Eq. D7 confirms the earlier research of Shields. Substituting $z = -\lambda_{ref}$, Eq. D7 can be given by

Figure D.2 Instability of grass cover (Bulging-mechanism)

$$\tau_0 \geq \tau_c = \Psi_c \left[(\rho_s - \rho) g \lambda_{ref} + 4\left(C_{clay,c} + \tau_{grass,c}\right) + \left(C_{clay,c} + \sigma_{grass,c}\left(-\lambda_{ref}\right)\right)\right] \quad \text{(D10)}$$

Soil can easily withstand pressure forces. The critical soil pressure is significantly higher than the critical soil tensile stress. Equation D10 represents the equilibrium equation for soils in which only vertical tensile forces are considered (Table D1). Provided the parameters $C_{clay,c}$, $\sigma_{grass,c}$ and $\tau_{grass,c}$ are known, the Shields approach based on a vertical balance of forces predicts not only the incipient motion of granular materials, but also the critical stage of both clayey and turf aggregates.

Material	Dimensions		Relevant strength
Cohesionless soils (saturated)			
sand	individual size	0.1 mm < d < 2 mm	submerged weight
gravel	individual size	2 mm < d < 64 mm	submerged weight
stones	individual size	d > 64 mm	submerged weight
Cohesive soils			
clay (saturated)	clayey aggregate	2 mm < d_{clay} < 50 mm	submerged weight / true cohesion
clay (unsaturated)	clayey aggregate	2 mm < d_{clay} < 50mm	true cohesion / suction strength
Grass cover (unsaturated)			
cemented sand (Vechtdijk)	turf aggregate	50 mm < λ_{ref} < 100 mm	root strength
clay	turf aggregate	50 mm < λ_{ref} < 100 mm	root strength / suction strength

Table D.1 Strength characteristics of cohesionless soils, cohesive soils and grass

References

Bezuijen, A, Köhler, H.-J., 1996. Filter and revetment design of water imposed embankments induced by wave and draw-down loadings. *Geosynthetics: Applications, Design and Construction*, Balkema, Rotterdam, The Netherlands.

De Groot, M.B., Andersen, K.H., Burcharth, H.F., Ibsen, L.B., Kortenhaus, A., Lundgren, H., Magda, W., Oumeraci, H., Richwien, W., 1996. Foundation design of caisson breakwaters, *Publication* 198. Norwegian Geotechnical Institute, Oslo, Norway.

Klar, M., 2005. Design of an endoscopic 3-D particle-tracking velocimetry system and its application in flow measurements within a grave layer, *Doctoral Thesis*, University of Heidelberg, Germany.

Van der Meer, J.W., 2008. Erosion strength of inner slopes of dikes against wave overtopping, Preliminary conclusions after two years of testing with the Wave Overtopping Simulator, Van der Meer Consulting, Marknesse, The Netherlands.

E Equilibrium of clayey aggregates

Considerable advances in predicting the equilibrium of clay has been made in the past decade (e.g. Yang 2006; Briaud et al. 1999, 2008). There are several mathematical models that can be used to predict the equilibrium of clay, but they are subject to great uncertainty unless detailed measurements of important parameters can be made. In particular, it is necessary to measure the critical mean bed shear stress. This Appendix only summarizes some basic processes involved in the equilibrium of clayey aggregates.

Although the equilibrium of clay depends on the water quality and the material history (saturation and weathering) the stability is mainly influenced by the macro-scale phenomena, that is, the magnitude of the clayey aggregates and the zones of weakness between the aggregates. Compacted clay has a high resistance to erosion and a low hydraulic conductivity (*K*), provided the clay is kept in sufficiently moist condition. However, in structured (or unsaturated) soil *K* is significantly higher due to the influences of the atmosphere, flora and fauna and varies from 10^{-5} m/s to 10^{-4} m/s (Kruse 1998). Therefore, τ_c varies from 2 N/m^2 (loose clayey soils or structured soil) to 25 N/m^2 (heavy clayey soils or compacted clay) (e.g Raudkivi 1998). For normal uniform flow conditions, i.e. for $r_0 = 0.1$, the critical flow velocity ranges from 0.5 m/s to 2 m/s. For high turbulence intensities ($r_0 = 0.2$) holds 0.25 m/s < U_c < 1 m/s.

Experiments by Mirtskhoulava (1988, 1991) have shown that in a water-saturated state, the equilibrium of clay with a natural structure is reached in successive stages. In the initial stage, elementary dispersed, loosened particles and aggregates separate and those with weakened bonds are washed away. This process leads to a rougher surface that may experience increased drag, frictional and lift forces on aggregates with a further increase of flow velocity due to local constricted flows. Higher fluctuating forces increase the vibration and dynamic action on the protruding aggregates. As a result, the bonds between aggregates are increasingly destroyed until larger aggregates are instantaneously torn out of the surface and carried away by the flow.

Assuming that the critical condition for moving aggregates is reached at the weakest spots the critical frictional forces on the side walls are neglected, thus the equilibrium of aggregates is based on the submerged weight and true cohesion at the contact areas (Fig. E1). If F_c equals zero then it follows from Eqs. D1 and D10 that τ_c for saturated clay at $z = -d_{clay}$ is

$$\tau_c = \Psi_c \left[\left(\rho_s - \rho \right) g d_{clay} + C_{clay,c} \right] \tag{E1}$$

where d_{clay} is the representative size of the aggregate near the bed. Combining $\tau_0 = 0.7\rho(r_0 U)^2$ and Eq. E1 and assuming that the flow is hydraulically rough, thus $r_0 > 0.05$ and for the condition of incipient motion $U_0 = U_c$, the critical depth-averaged flow velocity with Δ [= $(\rho_s - \rho)/\rho$] as the relative density, is

$$U_c = \alpha_0 r_0^{-1} \sqrt{\Psi_c \left(\Delta g d_{clay} + C_{clay,c} / \rho \right)} \tag{E2}$$

Based on the work of Mirtskhoulava (1988, 1991), Hoffmans and Verheij (1997) simplified the expression for cohesive sediments

$$U_c = \log\left(8.8h / d_a\right) \sqrt{0.4\left(\Delta g d_a + 0.6 C_{f,M} / \rho \right)} \tag{E3}$$

with

$$C_{f,M} = 0.035c \tag{E4}$$

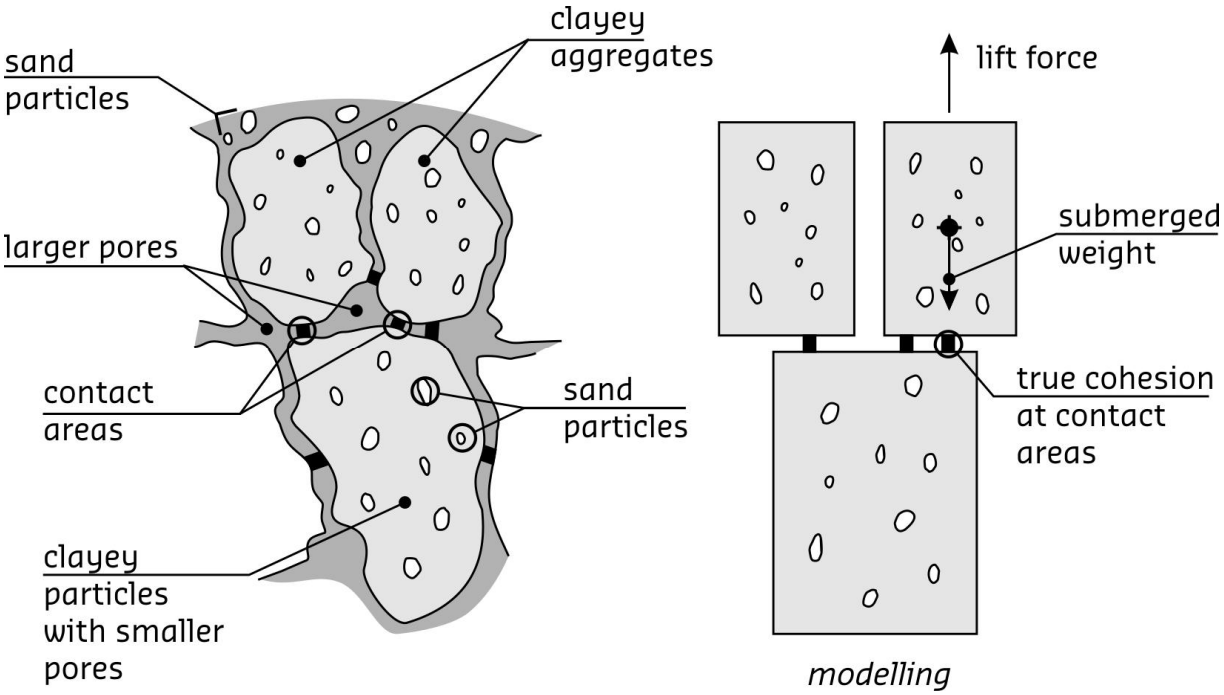

Figure E.1 Lifting of clayey aggregates

in which $C_{f,M}$ is the fatigue rupture strength of clay which is linearly related to the cohesion and d_a (= 0.004 m) is the characteristic size of detaching aggregates according to Mirtskhoulava (Table E1). By using $r_0 = 1.2\sqrt{g}/C$ and the Chézy coefficient, defined as

$$C = \left(\sqrt{g}/\kappa\right)\ln\left(12h/k_s\right) \tag{E5}$$

Eq. E3 becomes

$$U_c = \alpha_0 r_0^{-1}\sqrt{\Psi_{c,M}\left(\Delta g d_a + 0.6C_{f,M}/\rho\right)} \tag{E6}$$

with

$$\Psi_{c,M} = \left(\kappa/2.3\right)^2 \cdot 0.4 = 0.012 \tag{E7}$$

in which κ (= 0.4) is the constant of von Kármán and k_s (≈ 1.5 d_a) is the effective roughness. Hence, Eqs. E3 and E6 are similar. However, there are also differences between the cohesion parameters: $C_{clay,c} = 0.6C_{f,M}$, the representative aggregate diameters, d_{clay} and d_a and the critical Shields parameters, Ψ_c and $\Psi_{c,M}$. Assuming no cohesion, thus $C_{f,M} = 0$, it follows that Eq. E6 predicts minimal movement for aggregates with $d_a = d_{clay}$ = 4 mm, whereas Eq. E3 with Ψ_c = 0.033 calculates occasional movement at some locations. Therefore, the prediction of U_c by using the equation of Mirtskhoulava (1988, 1991) is certainly adequate for design purposes.

Cohesive soils retain water well and can be viscous and difficult to work with when wet. When dry, they typically shrink and crack. In some cases, structured soil will cause damage to roots. Structured soil contains cracks and thus the weakest spots are visible to the eye (Fig. E2). Under these conditions suction forces may increase the critical mean tensile force on the bottom element. If the weight of the aggregate is neglected with respect to the suction force, then the critical values of the mean bed shear stress and the depth-averaged flow velocity may be written as

$$\tau_c = \Psi_c C_{clay,c} \tag{E8}$$

and

$$U_c = \alpha_0 r_0^{-1}\sqrt{\Psi_c C_{clay,c}/\rho} \tag{E9}$$

with

$$C_{clay,c} = 0.6C_{f,m} = 0.6 \cdot 0.035c = 0.02c \tag{E10}$$

Consequently, the equations for τ_c and U_c are comparable for both saturated and unsaturated soils. Table E1 shows some indicative values of U_c for different qualities of clay under normal turbulence conditions (e.g. saturated clay at a riverbed, with r_0 = 0.1) as well as high turbulence conditions (e.g. structured soil on dike slopes with r_0 = 0.2). Note that small-scale erosion tests carried out in the laboratory may result in larger values of U_c because of the absence of weak spots and/or crack formation.

Quality of clay	[1] $C_{clay,c}$ (kN/m^2)	[2] U_c (m/s)	[3] U_c (m/s)
sand	-	< 0.4	< 0.2
poor	< 0.15	0.4 – 0.8	0.2 – 0.4
average	0.15 – 0.33	0.8 – 1.2	0.4 – 0.6
good	0.33 – 0.75	1.2 – 1.8	0.6 – 0.9
very good	> 0.75	> 1.8	> 0.9

[1] see also Eq. E10

[2] computed by using Eq. E9 with $\Psi_c = 0.03$ and $r_0 = 0.1$ (clayey river beds; normal turbulence conditions)

[3] computed by using Eq. E9 with $\Psi_c = 0.03$ and $r_0 = 0.2$ (structured soil on river dikes; high turbulence)

Table E.1 Indicative values of U_c and $C_{clay,c}$ for clayey aggregates

Figure E.2 Structured soil; clay can crack when dry

References

Briaud, J.-L, Ting, F.C.K., Chen, H. C., Gudavalli, R., Perugu, S., Wei, G., 1999. "SRICOS: Predictions of scour rate in cohesive soils at bridge piers", *J. Geotech. Geoenviron. Eng.*, 127(2), 105-113.

Briaud, J.-L, Chen, H,-C, Govindasamy, A.V., Storesund, R., 2008. Levee erosion by overtopping in New Orleans during the Katrina hurricane, *J. of Geotechnical and Geoenvironmental Engrg*., ASCE, 134(5), 618-632.

Hoffmans, G.J.C.M., Verheij, H.J., 1997. *Scour manual*, Balkema, Rotterdam.

Kruse, G., 1998. Impact of weathering on resistance of soils, in *Dikes and revetments, Design, Maintenance and Safety Assessment* (edt. K.W. Pilarczyk), Balkema, Rotterdam.

Mirtskhoulava, Ts. Ye., 1988. *Basic physics and mechanics of channel erosion*, Gidrometeoizdat, Leningrad.

Mirtskhoulava, Ts. Ye., 1991. Scouring by flowing water of cohesive and non cohesive beds, *J. Hydr. Res.*, 29(3), 341-354.

Raudkivi, A.J., 1998. *Loose boundary hydraulics*, Balkema, Rotterdam.

Yang, C.T., 2006. Erosion and sedimentation manual. U.S. Department of the Interior Bureau of Reclamation, Technical Service Center Sedimentation and River Hydraulics Group. Denver, Colorado.

F Equilibrium of turf aggregates

Grass can easily resist flow velocities of up to 2.0 m/s. Higher velocities can also be withstood. However, the critical value depends strongly on the root qualities and the changes of the suction pressures as discussed in Chapter 5. The mean grass strength is a function of the root area ratio, the mean root diameter and the critical mean root tensile stress. Prototype experiments carried out on Dutch dikes showed that the stability of a larger area of the grass cover may influence the failure of the inner slope. If the soil in the grass cover is saturated and if both the submerged weight and the strength of clay are neglected with respect to the strength of grass, then Eq. D10 reduces to

$$\tau_0 \geq \tau_c = \Psi_c \left[4\tau_{grass,c} + \sigma_{grass,c}\left(-\lambda_{ref}\right) \right] \tag{F1}$$

The relevant strength is then determined by the roots, both at the side walls (frictional strength) and at the bottom (tensile strength). Owing to the intersected roots, the critical mean grass shear stress averaged over λ_{ref} is per side wall (see also Eq. C5)

$$\tau_{grass,c} = \frac{1}{\lambda_{ref}} \int_{-\lambda_{ref}}^{0} \sigma_{grass,c}\left(z\right) \mathrm{d}z$$

or

$$\tau_{grass,c} = \frac{\sigma_{grass,c}\left(0\right)}{\lambda_{ref}} \int_{-\lambda_{ref}}^{0} \exp\left(\frac{z}{\lambda_{ref}}\right) \mathrm{d}z$$

or

$$\tau_{grass,c} = \alpha_{grass} \sigma_{grass,c}\left(0\right) \tag{F2}$$

with

$$\alpha_{grass} = 1 - \exp\left(-1\right) = 0.64 \tag{F3}$$

Note that $\tau_{grass,c}$ and $\sigma_{grass,c}(0)$ do not depend on the magnitude of λ_{ref}. Combining Eqs. F1, F2 and F3 yields

$$\tau_0 \geq \tau_c = \alpha_{grass,\tau} \Psi_c \sigma_{grass,c}\left(0\right) \tag{F4}$$

with

$$\alpha_{grass,\tau} = \left(1 + 3\alpha_{grass}\right) = 2.9 \tag{F5}$$

Assuming that the flow is hydraulically rough, thus $r_0 > 0.05$ and for the condition of incipient motion $U_0 = U_c$, the critical depth-averaged velocity for grass is

$$U_c = \alpha_{grass,U} r_0^{-1} \sqrt{\Psi_c \sigma_{grass,c}\left(0\right) / \rho} \tag{F6}$$

with

$$\alpha_{grass,U} = \alpha_0 \sqrt{\left(1 + 3\alpha_{grass}\right)} = 2.0 \tag{F7}$$

With the assumptions $r_0 = 0.2$, $d_{root} = 0.1$ mm, $\theta = 60^o$, $\phi = 30^o$, $\sigma_{root,c} = 15 \cdot 10^6$ N/m^2, and $\Psi_c = 0.03$, the following values for U_c are obtained for different qualities of grass (Table F1).

The Vechtdijk, a Dutch dike along the river Vecht, consists of about 90% sand. The erodibility of the grass cover was tested during the winter season 2010 when roots usually are at their weakest strength. However, the root investigation showed that the number of roots and the cover ratio were still qualified as “good”. During the experiments the sand in the top soil was cemented giving the turf aggregate sufficient strength for compression which is required since the load of overtopping waves generates over pressures as well as under pressures.

Because of the relatively high permeability of sand, the infiltrated water resulting from overtopping waves reduces the suction pressure almost at once in both the larger and smaller pores. Therefore, after infiltration the apparent cohesion is probably negligible in and under the turf layer. On the sandy Vechtdijk, experiments in which the significant wave height varied (H_s = 1 m, 2 m and 3 m) showed that $U_c \approx 4$ m/s was needed to give similar results. Table F1 demonstrates that the value of U_c is about 4.5 m/s for good grass which agrees reasonably well with the results of the cumulative effective load model as developed by Van der Meer et al. (2010). Suction pressures in unsaturated soils may increase the strength of the top soil. Including these effects Eq. F6 can be given by

$$U_c = \alpha_{grass,U} r_0^{-1} \sqrt{\Psi_c \left(\sigma_{grass,c}(0) - p_w \right) / \rho} \qquad \text{(F8)}$$

The pore water pressure, which has a negative sign, represents the suction pressure in the roots and clay aggregates, which decreases with time after infiltration. If the contribution of suction pressures is taken into account, for example if the sand dike is covered with clay, thus if p_w = –10 kN/m^2, then the value of U_c could reach values up to 7 m/s for good grass (Table F1). If p_w = –5 kN/m^2 then $U_c \approx 6$ m/s. Hence, the magnitude of the suction pressures influences U_c significantly.

Quality of grass	[1] $\sigma_{grass,c}(0)$ (kN/m^2)	[2] U_c (m/s)	[3] U_c (m/s)
very poor	< 3.0	< 3.0	< 6.2
poor	3.0 – 5.3	3.0 – 4.0	6.2 – 6.8
average	5.3 – 7.5	4.0 – 4.7	6.8 – 7.2
good	> 7.5	> 4.7	> 7.2

[1] see also Table 5.2

[2] computed by using Eq. 5.43 with p_w = 0 kN/m^2, r_0 = 0.2 (steepness of slope is about 1V:3H) and Ψ_c = 0.03

[3] computed by using Eq. 5.43 with p_w = –10 kN/m^2, r_0 = 0.2 and Ψ_c = 0.03

Table F.1 Indicative values of U_c and $\sigma_{grass,c}(0)$ for grass (high turbulence)